Reveal of Vision Transformers Robustness against Adversarial Attacks

Ahmed Aldahdooh, Wassim Hamidouche, and Olivier Déforges

Abstract—The major part of the vanilla vision transformer (ViT) is the attention block that brings the power of mimicking the global context of the input image. For better performance, ViT needs large-scale training data. To overcome this data hunger limitation, many ViT-based networks, or hybrid-ViT, have been proposed to include local context during the training. The robustness of ViTs and its variants against adversarial attacks has not been widely investigated in the literature like CNNs. This work studies the robustness of ViT variants 1) against different L_p-based adversarial attacks in comparison with CNNs, 2) under adversarial examples (AEs) after applying preprocessing defense methods and 3) under the adaptive attacks using expectation over transformation (EOT) framework. To that end, we run a set of experiments on 1000 images from ImageNet-1k and then provide an analysis that reveals that vanilla ViT or hybrid-ViT are more robust than CNNs. For instance, we found that 1) Vanilla ViTs or hybrid-ViTs are more robust than CNNs under L_p-based attacks and under adaptive attacks. 2) Unlike hybrid-ViTs, Vanilla ViTs are not responding to preprocessing defenses that mainly reduce the high frequency components. Furthermore, feature maps, attention maps, and Grad-CAM visualization jointly with image quality measures, and perturbations' energy spectrum are provided for an insight understanding of attention-based models.

Index Terms—Vision transformer, convolutional neural network, robustness, adversarial attacks, deep learning.

◆

1 INTRODUCTION

IMAGE classification task models have remarkable progress in its prediction accuracy especially when convolutional blocks serve as the main building block of the model [1]. Convolutional blocks have the ability to exploit the spatial features and in particular the low-level features [2]. On the other hand, self-attention blocks in Transformers [3] showed great success in natural language processing (NLP) models [3], and recently, Dosovitskiy *et al.* proposed vision transformer (ViT), vanilla ViT, the first image classification model that uses the pure transformer encoder blocks [4] and image patches, as tokenization, to build the classifier. To overcome the lack of the inductive biases inherent to convolutional neural networks (CNNs), it was shown that ViT achieves better performance than state-of-the-art CNNs models of similar capacity, such as ResNet [1] and its variants if ViT is trained with significantly large-scale training datasets, such as JFT-300M [4], [5]. Moreover, ViT models that are trained on large-scale datasets can be downgraded to smaller datasets, such as ImageNet-1k [6], via transfer learning, leading to performance comparable to or better than state-of-the-art CNNs models. Given the advantage of the ViT and on the other side its limitation to the huge need of the data, other models that combine the vanilla ViT with other modules, like tokens-to-token ViT (T2T-ViT) [2], transformer-in-transformer (TNT) [7], and CvT [8] models

were proposed for better learning the low-level features in the transformer and hence, reduce their dependency on large datasets. These models are also known as hybrid-ViT models

Given many CNN image classification task models [1], [9], [10], [11], their properties are well studied and analyzed including the robustness against adversarial examples (AEs) [12]. AE is a combination of the original image and a carefully crafted perturbation [12]. This perturbation is hardly perceptible to humans, while it causes the deep learning (DL) model to misclassify the input image. Since the feature space identification of the AE is hard to predict [13], [14], the adversarial attacks threat is very challenging. Adversary can generate AEs under white box, black box, and gray box attack scenarios [15], [16].

Due to the success of ViT and its variants in various computer vision tasks, the insight properties and robustness studies for such transformers are yet under investigation. Recently, four studies [17], [18], [19], [20] showed some of these robustness properties for the vision transformers and compared them with the competitive CNN models. In this work, we experimentally investigate the robustness of different ViT variants against different L_p-based and color channel perturbations (CCP) attacks and their strength of predicting the preprocessed AEs, as defense. The results are compared with competitive CNN models. We attend to answer the following research questions 1) Are ViT variants more robust than CNNs against L_0, L_1, L_2, and L_∞ based attacks and against CCP attack? 2) Are ViT variants more robust than CNNs under the preprocessed AEs? 3) Is increasing the number of attention blocks has an effect on the robustness against the AEs and under the preprocessed AEs? 4) Is enhancing ViT tokenization method has an effect on increasing the robustness against the AEs and under the preprocessed AEs? Hence, this work will provide researchers

- All authors are with INSA Rennes, CNRS, IETR - UMR 6164, University of Rennes, 35000, Rennes, France.
- Corresponding author: A. Aldahdooh, E-mail: ahmed.aldahdooh@insa-rennes.fr

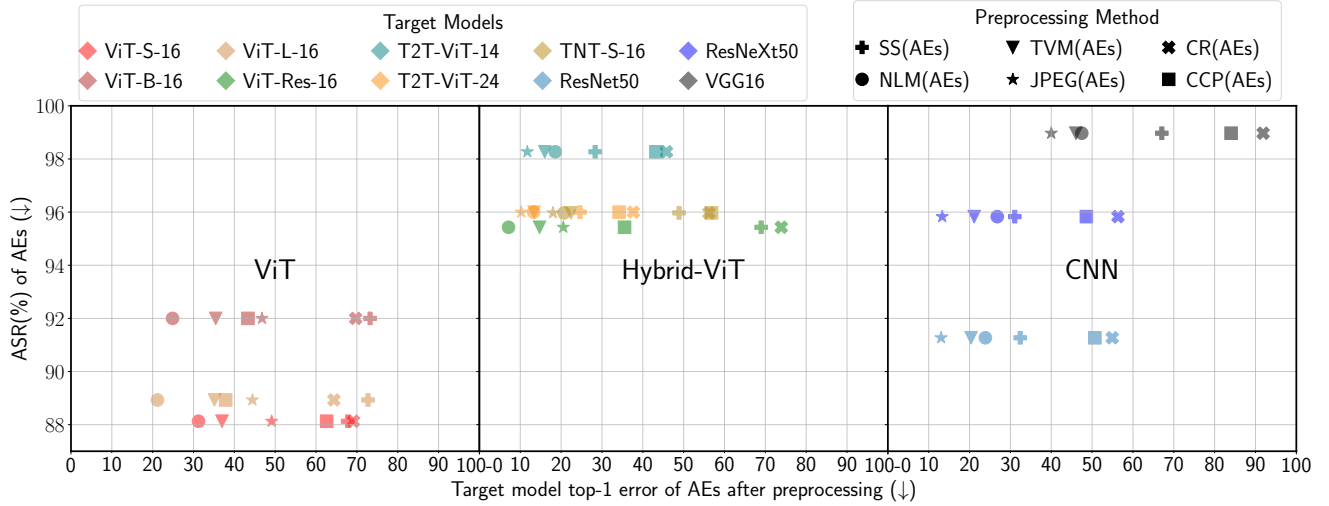arXiv:2106.03734v2 [cs.CV] 20 Sep 2021

Fig. 1: The attack success rate (ASR) of target models, on 1000 images from ImageNet-1k, against AutoAttack, in average $\epsilon = \{1, 2, 4\}/255$, and the target model top-1 error of the preprocessed AEs for six different preprocessing defense methods including SS: local spatial smoothing, NLM: non-local mean, TVM: total variation minimization, JPEG: JPEG compression, CR: cropping and re-scaling and CCP: color channel perturbations.

with an in-depth understanding on how vision transformers behave against different attack settings with preprocessing defenses, see Figure 1. The main contribution of this work is to highlight the following observations:

- ViT-based models are more robust than CNNs against L_p-norm attacks.
- Neither larger model's architecture, like ViT-L, nor bringing convolutional modules for tokenization in ViTs, like TNT, will necessarily enhance the robustness.
- In general, transferability exists within the model architecture family and the transferability became lower when transfer from large to small variants and vice versa.
- Black-box attacks are transferable to CNNs when they are generated using vanilla ViTs and hybrid-ViTs and not vice versa.
- Vanilla ViTs are not responding to preprocessing defenses that mainly reduce the high frequency components, such as local spatial smoothing (SS) and JPEG compression (JPEG). Hybrid-ViTs are more responsive to preprocessing defenses than vanilla ViTs and CNNs, see Figure 1.
- Hybrid-ViT models show better robustness than vanilla ViTs and ResNets under the expectation over transformation (EOT) robustness test.

2 RELATED WORK

Robustness of computer vision CNNs against AEs is well studied in the literature [12], and many countermeasures [15], [16], [21], [22], [23], i.e. defenses and detectors, were implemented to characterize the feature space of the AEs. On the other hand, self-attention based computer vision models are under investigation. The work in [24] used vanilla self-attention transformer to improve the object detection task detector's robustness against AEs. The new module used the self-attention transformer to model the features that are extracted from fast region convolutional neural network (Fast-RCNN) [25] before running the detection classifier. Recently, four studies [17], [18], [19], [20] provided some

understanding of the robustness of ViT, and its variants. Authors in [17], [19], [20] studied the robustness of the vanilla ViTs, while the work in [18] studied the robustness of vanilla ViTs and of other models that combine vanilla ViT with other modules like convolutional blocks, hybrid-ViTs. The work in [17] investigated the ViT robustness with respect to the perturbations of both the input and model. The study of input perturbations included natural corruption, real-world distribution shifts, natural adversarial perturbations, adversarial attack perturbations, adversarial spatial perturbations, and texture bias. The adversarial attack perturbations are generated using L_∞ bounded (ϵ) AEs using fast gradient sign method (FGSM) [26] and projected gradient descent (PGD) [27] attacks where ϵ was set to one gray-level (1/255). The input perturbations are tested on models that are pretrained on ImageNet-1k [6], ImageNet-21k [28], and JFT-300M [5] datasets. It was shown that, like CNNs, ViTs are vulnerable to AEs and it is more robust than CNNs with comparable capacity when trained on sufficient training data. Similarly, the work in [19] investigated the robustness of ViT and big transfer (BiT) CNN [29] against common corruptions and perturbations, distribution shifts, and natural adversarial examples. The work in [18] showed that this observation is not necessarily true and claimed that the robustness of ViT is more related to transformer architecture rather than the pretraining. In [18], it was shown that introducing convolutional blocks or tokens-to-token [2] modules compromises the model robustness when tested against L_∞ PGD [27] and auto projected gradient descent (Auto-PGD) [30] attacks. Moreover, [18] showed that CNNs are less robust than ViTs since CNN tends to learn low-level features that are much vulnerable to adversarial perturbations. The three works in [17], [18], [19] showed that AEs do not transfer across different model architectures' families which leads to have an ensemble models approach to defend against the attacks. Hence, the work in [19], included more L_∞ attacks like; Carlini-Wagner (CW) [31], momentum iterative gradient-based method (MI-FGSM) [32], and backward pass differentiable approximation (BPDA) [33], and focused on the transferability of the attacks to introduce the self-attention

gradient attack (SAGA) that can fool the ensemble defense model. In this work, we investigate the robustness against different L_p norms attacks and the robustness under the pre-processed AEs, as a defense technique.

3 PRELIMINARIES

3.1 Models' architectures

In this section, a brief description of models that are investigated in our experiments is introduced. Table 1 gives the parameters of the investigated models[1].

Vanilla transformer [4]. The vanilla self-attention Transformer was introduced for NLP tasks. It stacks the encoder and the decoder blocks, where each block stacks N attention blocks. The attention block has two sub-layers. The first one is a multi-head self-attention mechanism, and the second one is a simple, position-wise fully connected feed-forward network. The residual connection around each of the two sub-layers followed by layer normalization are employed. Encoder and decoder input tokens are converted to a sequence of vectors using learned embeddings. Finally, the learned linear transformation and *softmax* function are used to convert the decoder output to predict next-token probabilities.

Vision transformer (ViT) [4]. It is the first model that employed the vanilla transformer architecture and achieved state-of-the-art performance on image classification task. To adapt the vanilla transformer for image classification, ViT 1) divides the input image into a sequence of patches and then linearly projects them to the transformer, 2) appends [CLS] token to the input and output representations that are passed to multi-layer perceptron (MLP) for the classification task. In our investigation, we consider different ViT models including ViT-S/B/L-16 models. In the single-head self-attention (SHSA) of ViTs [4], each image $X \in \mathbb{R}^{n \times d}$ is presented as a sequence of n patches $(x_1, x_2, \ldots x_n)$, where d is the embedding dimension to represent each patch. Then, the image sequence, X, is linearly projected onto query ($Q = XW_q$), key ($K = XW_k$), and value ($V = XW_v$), where $W_q \in \mathbb{R}^{d \times d_q}$, $W_k \in \mathbb{R}^{d \times d_k}$, and $W_v \in \mathbb{R}^{d \times d_v}$. In this way, the image patch is encoded in terms of the global information, which enables the self-attention structure mechanism to capture the interactions among image patches. By applying scaled dot-product attention mechanism, the output of one self-attention Z is computed as:

$$Z = Attention(Q, K, V) = \textbf{softmax}\left(\frac{QK^T}{\sqrt{d_k}}\right)V. \quad (1)$$

According to (1), firstly, the attention scores of input query and key are calculated, $S = QK^T$, which is then normalized by $\sqrt{d}$ to prevent pushing the **softmax** function into regions where it has extremely small gradients when d becomes large. Then, the probabilities of the normalized scores are calculated, $P = \textbf{softmax}(S/\sqrt{d})$. Finally, the value vector V is multiplied by the probabilities P to calculate Z in which larger probabilities are the focus in the following layers.

The SHSA limits the capability to highlight the importance of other equally important patches at the same time.

Having multi-head self-attention (MHSA) can mitigate this problem by having different Q, K, and V vectors for each self-attention, and hence, can jointly attend to information from different representation subspaces at different positions. In MHSA, the Q, K, and V have the size of $X \in \mathbb{R}^{n \times d/h}$, where h is the number of heads, and $d_q = d_k = d_v = d/6$. Hence, the output of MHSA has the output of size $X \in \mathbb{R}^{n \times d}$ and is calculated as follows:

$$MultiHead(Q', K', V') = (head_1 \oplus \cdots \oplus head_h)W^o,$$
$$head_i = Attention(Q_i, K_i, V_i), \, \forall i \in \{1, \cdots, h\}, \quad (2)$$

where Q', K', V' are the concatenation of $\{Q_i\}_{i=1}^h$, $\{K_i\}_{i=1}^h$, and $\{V_i\}_{i=1}^h$ respectively, and $W^o \in \mathbb{R}^{d \times d}$ is the linear projection matrix. $\oplus$ stands for vector concatenation operation.

The ViT's encoder block stacks N layers of attention blocks. The attention block has two sub-layers. The first one is a MHSA, and the second one is a simple MLP layer, also known as position-wise fully connected feed-forward network (FFN). Layernorm (LN) is applied before every sub-layer, and residual connections are applied after each sub-layer. This latter consists of two linear transformation layers and a nonlinear activation function, Gaussian error linear units (GELU) [34], in between.

The work in [18] showed that the fact of having ViTs trained on large-scale dataset yield to more robust models than CNNs is not necessarily true and claimed that the robustness of ViTs is more related to transformer structure rather than the pre-training. Hence, in our investigation, Vanilla ViTs are pretrained on ImageNet [28] and fine-tuned on ImageNet-1k [6], while hybrid-ViTs and CNN are trained from scratch on ImageNet-1k.

Hybrid-ViT models [2], [4], [7]. One key of CNNs success is the ability to learn local features, while the key success of self-attention based transformer is its ability to learn the global features. Hence, many approaches were introduced to integrate local feature representation in ViT model. The work in [4], replaced input image patches with the CNN feature map patches and introduced ViT-Res that used the flattened ResNet feature maps to generate the input sequence. In [2], tokens-to-token ViT (T2T-ViT) is introduced. It replaces input image patches with a layer-wise tokens-to-token (T2T) transformation, then, the features that are learned by T2T module are passed to the ViT. The aim of T2T module is to progressively structurize the image into tokens by recursively aggregating neighboring tokens into one token. The work in [7] proposed a transformer-in-transformer (TNT) architecture to model both patch-level and pixel-level representations. The TNT is made up by stacking TNT blocks. Each TNT block has an inner transformer and an outer transformer. The inner transformer block extracts local features from pixel embeddings. In order to add the output of the inner transformer into the patch embeddings, the output of the inner transformer is projected to the space of patch embedding using a linear transformation layer. The outer transformer block is used to process patch embeddings. In our investigation, we consider T2T-ViT-14/24, and TNT-S-16 models.

Convolutional neural network (CNN). The convolutional layer is the basic building block for the CNN models. It has a set of learnable small receptive field filters. These filters

---

1. The weights are available here , for all models except for T2T-ViTs which are available here.

TABLE 1: ViT, ViT-based, and CNN model variants that are investigated in this work.

Category	Model	ViT Backbone			Params (M)	Top-1 Acc.(%) on ImageNet-1k
		Layers	Hidden size	MLP size		
Vanilla ViT†	ViT-S-16 [35]	8	786	2358	49	77.858
	ViT-B-16 [4]	12	786	3072	87	81.786
	ViT-L-16 [4]	24	1024	4096	304	83.062
Hybrid-ViT*	ViT-Res-16 (384) [4]	12	786	3072	87	84.972
	T2T-ViT-14 [2]	14	384	1152	22	81.7
	T2T-ViT-24 [2]	24	512	1536	64	82.6
	TNT-S-16 [7]	12	384	1536	24	81.518
		CNN Backbone Conv. Layers				
CNN*	ResNet50 [1]	49			23	79.038
	ResNet50-32x4d (ResNeXt50) [36]	49			25	79.676
	VGG16 [9]	13			138	71.594

† Pre-trained on ImageNet-21k [28] and fine tuned on ImageNet-1k [6],
* Trained from scratch on ImageNet-1k [6]

are convolved across the full depth of the input to produce the feature maps. Hence, feature maps can remarkably represent local structure of the input image. Many architectures have been proposed in the literature [37]. In our investigation, we consider ResNet50 [1], ResNeXt50_32x4d [36], and VGG16 [9] models.

3.2 Adversarial attacks

Our investigation assumes that the adversary can create an AE x' by perturbing the input image x with a certain amount of noise ϵ, such that $||x - x'||_p \leq \epsilon$, where $p \in \{0, 1, 2, \ldots, \infty\}$, under different attack scenarios; white-, black-, hybrid-, and gray-box attacks. We investigate the target models with 1000 images that are correctly classified by all the target models. The test samples are collected from ImageNet-1k validation dataset [6]. Our investigation, included five white-box attacks: jacobian saliency map attack (JSMA) [38], FGSM [26], PGD [27], universal adversarial perturbations (UAP) [39], and CW [31]. For the black-box attacks, we consider square attack (SA) [40], ray searching (RayS) [41], and CCP [42] attacks. Moreover, we consider autoattack (AA) [30], as hybrid-box attack, which is an ensemble attack that runs three attacks to generate the AEs: the Auto-PGD, acfab [43], and SA. For the gray-box attacks, the adversary has knowledge about training data but not the model architecture and depends on the transferability property of the attacks to generate the AEs using a surrogate model. Given the surrogate model, the aforementioned attacks can be used to generate AEs. In our investigation, one of our target models will be considered as a surrogate model to generate the AEs and these AEs will be tested on the other target models. Table 2 lists the attack's parameters that are used in our experiments. All the attacks are generated using adversarial robustness toolbox (ART)[2], except RayS attack that is generated using the official implementation [3].

In [18], a preliminary results were introduced to train robust ViT classifiers using adversarial training (AT). It is stated that "ViT does not advance the robust accuracy after adversarial training compared to large CNNs such as

WideResNet-34-10". That is because ViT may need larger training data or longer training epochs to further improve its robust training performance. Moreover, it is found that AT can still cause catastrophic overfitting for ViT when fast AT training is conducted, to mitigate the overfitting, with FGSM, further adjustments were needed to propose AT for ViT. Due to such reasons we couldn't conduct a fair AT comparison with CNN and we left it as future work.

3.3 Pre-processing defense methods

We consider pre-processing methods that were previously applied to the AEs before being forwarded to the CNNs in order to alleviate the effect of added perturbations. In our investigation, we consider local smoothing [44], non-local mean denoising [44], total variation minimization [45] , JPEG image compression [46], [47], and crop and re-scaling [48].

Local smoothing [44]. Is a method that uses a pixel neighborhood to smooth out each pixel. For a given $n \times n$ sliding window, local smoothing changes each pixel, center of the sliding window, with the mean, the median, or Gaussian smooth of the window. In [44], it was shown that median filter is more efficient in projecting the AE back to the data manifold especially for L_0 based attacks, since it is capable of removing sparsely pixels in the input image, and at the same time it preserves edges. In our investigation we use the median filter with 3×3 window size.

Non-local mean denoising [44]. As the name indicates, the non-local smoothing not only uses the nearby pixels, but uses several similar patches within a search window, as well, to smooth out the current patch. While preserving image edges, it is assumed that averaging similar patches to smooth the current patch will remove the perturbations when the mean of the noise is zero. In our investigation, we use the patch size of 7×7 and the search window of 23×23 and the strength of 0.07. We use **skimage** restoration library to run the non-local mean denoising. For each noisy image, i.e. the AE, the robust wavelet-based estimator of the Gaussian noise standard deviation is used before applying the non-local mean (NLM) denoiser [49].

Total variation minimization [45]. Total variation denoising was shown to be effective in removing adversarial

TABLE 2: Considered adversarial attacks and their parameters.

Scenario	Attack	norm	Parameters
White box	FGSM	L_∞	$\epsilon \in \{1, 2, 4, 8, 16, 24\}/255$
	PGD	L_1	$\epsilon \in \{100, 150, 200, 400, 600, 800, 1000\}$, $\epsilon_{step} = \epsilon/10$, *max. iterations*=10
	PGD	L_2	$\epsilon \in \{0.5, 1, 2, 3, 4, 5\}$, $\epsilon_{step} = \epsilon/10$, *max. iterations*=10
	PGD	L_∞	$\epsilon \in \{1, 2, 4\}/255$, $\epsilon_{step} = \epsilon/10$, *max. iterations*=10
	CW	L_2	*max. iterations*=10, *learning rate*=5e-3, *initial const*=2/255, *binary search steps*=10
	CW	L_∞	$\epsilon = 8/255$, *confidence*=0, *max. iterations*=50, *learning rate*=5e-3
	UAP	L_∞	$\epsilon \in \{1, 2, 4\}/255$, *attacker*=BIM, $\epsilon_{step} = \epsilon/10$, *max. iterations*=10
	JSMA	L_0	$\theta = 0.1, \gamma = 1$,
Black box	SA	L_∞	$\epsilon \in \{8, 16\}/255$, $p = 0.05$, *max. iterations*=300, *restarts*=1
	RayS	L_∞	$\epsilon = 8/255$, *query*=2000
Hybrid box	AA	L_∞	$\epsilon \in \{1, 2, 4\}/255$
Other Attacks	CCP	-	*seed*=0 for fixed random-weight based CCP attack, $s = 2$ and $b = 30$.

perturbations due to its ability to minimize the total variation of the image by producing similar images to the noisy images. It was shown that total variation simultaneously preserves edges and denoises flat regions. We use the Chambolle algorithm [50] that is implemented in **skimage** library with strength of 0.1 and $\epsilon = 2e - 4$.

JPEG image compression [46], [47]. Compression is used to remove redundancy in images by removing high frequency components that are imperceptible to humans. On the other hand, adversarial perturbation is imperceptible and hence it is assumed that the high frequency details of the image are more vulnerable to adversarial perturbations. In our experiments, we compress the AEs at quality level of 65%.

Cropping and re-scaling [48]. It was shown that image cropping and re-scaling method is an effective way to remove the adversarial perturbations effect due to the spatial re-positioning of the pixels. This method may harm the structure of the carefully crafted adversarial perturbations. We perform center cropping with 2-pixel margin for top, bottom, left, and right of the image, and then re-scale the cropped image to the input size.

Finally, it is worth mentioning that the pre-processing defense can be easily fooled using BPDA [33] and EOT [51] techniques. In our investigation, we consider the EOT attack to have a deep insight in the robustness of the ViTs based models.

3.4 Analysis tools

We rely our investigations on tools that can reveal the properties of the model's behavior such as feature [2], attention [4], and gradient-weighted class activation mapping (Grad-CAM) [52] maps. Moreover, we use discrete cosine transform (DCT) based decomposition of the perturbations [53] and the visual quality assessment of the AE [54] as tools to assess the robustness of target models against the AEs. We consider three objective visual quality assessment metrics including peak signal to noise ratio (PSNR), structural similarity index measure (SSIM) [55], and most apparent distortion (MAD) [56].

Feature and attention maps: In [2], a visualization method to visualize the feature maps for CNNs and ViTs is recommended. For simplicity, we get the feature maps of clean and adversarial samples and then visualize the

difference of one channel only, randomly selected, and finally normalize it to [0, 1] scale. As recommended in [2], input sample is upsampled to clearly visualize the ViT feature maps. To visualize the attention map, we follow the rollout-based attention visualization method that is provided by [4] and implemented in the ViT-pytorch github repository[4].

Grad-CAM [52] uses the gradients of any target class flowing into the final convolutional layer to produce a coarse localization map highlighting the important regions in the image in the class prediction. Since convolutional blocks are missing in ViTs, [57] uses the LN output of the last attention block to calculate the gradients and then [57] reshapes the activation and gradients to 2D spatial images to fit the Grad-CAM algorithm.

DCT-based decomposition of perturbations. In [53], it was shown that construction of the class decision boundary is extremely sensitive to small perturbations of the training samples. Moreover, it was shown that CNNs mainly exploit discriminative features in the low frequencies of MNIST, CIFAR-10, and ImageNet-1k datasets. This explains why, in some query-based black-box attacks like in [58], using low-frequency perturbations improves the efficiency of the attack's query. To show how we take advantage of this observation in our investigation, we consider the DCT de-composition of the perturbations for non norm-constrained[5] attacks, like CW attacks, and for norm-constrained attacks, like FGSM and PGD-based attacks as shown in Figure 2 and Figure 3, respectively. For ResNet, it is very clear that the perturbations' discriminative features are more centered around low frequency components. While, for ViTs, the perturbations' discriminative features are spread in all frequency spectrum region. We conclude that, the wider the spread of perturbations' discriminative features the more robust the model against the attacks, because the adversarial attack algorithms have to affect a wider range of frequency spectrum.

PSNR. It is the most widely used metric because it is simple and mathematically convenient for optimization.

---

4. https://github.com/jeonsworld/ViT-pytorch

5. In [53], to measure perturbation distance to the decision boundary, they found that non norm-constrained attacks are more suitable for the study. In our experiments, we show that, for ResNet, the perturbations' discriminative features are more centered around low frequency in non norm-constrained attacks.
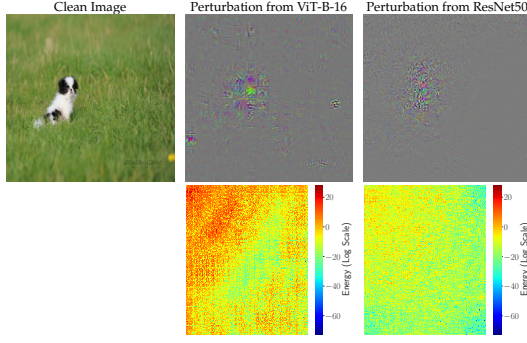
Fig. 2: The perturbation (top), generated using CW-L_∞ attack with ViT-B-16 (middle) and ResNet50(left), and the corresponding DCT-based spectral decomposition heatmap. Perturbation is scaled from [-1, 1] to [0, 255].

Fig. 3: The perturbation (top), generated using PGD-L_∞ $\epsilon = 4/255$ attack with T2T-ViT-14 (middle) and ResNet50(left), and the corresponding DCT-based spectral decomposition heatmap. Perturbation is scaled from [-1, 1] to [0, 255].
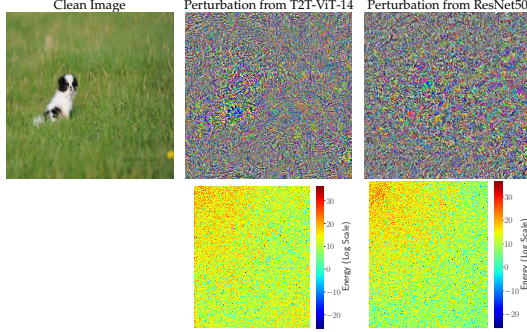
Unfortunately, PSNR doesn't correlate well with human perception. It is calculated as:

$$PSNR = 10 \, log_{10} \left(\frac{MAX^2}{MSE} \right)$$
$$MSE = \frac{1}{N} \sum_{i=1}^{m} \sum_{j=1}^{n} [x(i,j) - x'(i,j)]^2, \quad (3)$$

where MAX is the maximum density value, $2^8 - 1$ in 8-bit images, MSE is the mean squared error, m and n are the image width and height, $N = mn$, and PSNR $\in [0, \infty[$. The higher the PSNR the better the quality and $PSNR \to \infty$ means that the two images are identical.

SSIM [55]. It is a full reference image quality metric that relies on the fact that the human visual system (HVS) highly tends to extract structural information from the image. SSIM extracts information that is related to the luminance (l), the contrast (c), and the structure (s) from two images, here x and x', and measures the similarity between them as:

$$SSIM(x, x') = l(x, x')c(x, x')s(x, x')$$
$$= \frac{(2\mu_x\mu_{x'} + c_1)(2\sigma_{xx'} + c_2)}{(\mu_x^2 + \mu_{x'}^2 + c_1)(\sigma_x^2 + \sigma_{x'}^2 + c_2)}, \quad (4)$$

where μ_x is the average of x, $\mu_{x'}$ is the average of x', σ_x is the variance of x, $\sigma_{x'}$ is the variance of x', $\sigma_{xx'}$ is the covariance of x and x', and c_1 and c_2 are hyperparameter to avoid instability when denominator is close to zero. The range of SSIM is $[0, 1]$, where SSIM = 1 means that the two images are identical. In our experiments, we assume that the
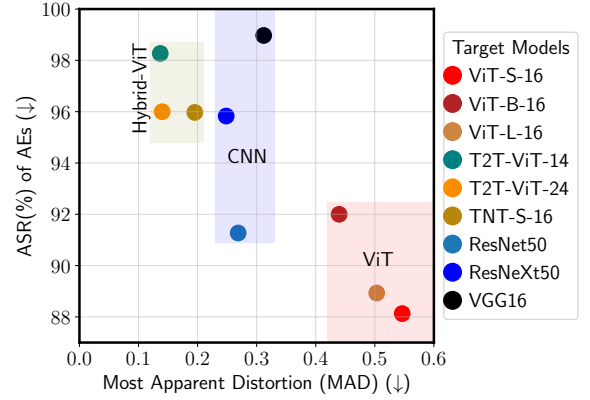

Fig. 4: The attack success rate (ASR) of target models, on 1000 images from ImageNet-1k against AutoAttack, in average $\epsilon = \{1, 2, 4\}/255$, and the most apparent distortion (MAD)

target model $\mathcal{M}$ is more robust than other models if the AE that is generated using the $\mathcal{M}$ has lower SSIM score than other models because the adversarial attack algorithm has to generate AE with higher perturbation that influences the structure of the AEs.

MAD [56]. Adversary usually generates AE that are imperceptible to human as much as they can by adding perturbations that are near threshold distortions. On the other hand, MAD attempts to explicitly model two strategies employed by the HVS. The first one is a detection-based strategy for high-quality images containing near threshold distortions[6] that are typical situation for AEs with low perturbation. The second one is an appearance-based strategy for low-quality images containing clearly suprathreshold distortions, that are typical situation for AEs with high perturbation. As stated in [56], local luminance and contrast masking are used to estimate detection-based perceived distortion in high-quality images, whereas changes in the local statistics of spatial-frequency components are used to estimate appearance-based perceived distortion in low-quality images. Moreover, it was shown in [54] that MAD has better correlation to subjective scores for AEs. The range of MAD score is $[0, \infty]$ where MAD = 0 is close to the clean image. In our experiments, we assume, as shown in Figure 4, that the target model $\mathcal{M}$ is more robust than other models if the AE that is generated using the $\mathcal{M}$ has higher MAD score than other models because the adversarial attack algorithm don't be able to prevent the perception of the perturbation.

4 REVEAL OF THE ROBUSTNESS ATTRIBUTES

4.1 General observation

In Figure 5 and Figure 7, for instance, the first row shows the AEs, while the top row of Figures 5b and 7b, and Figures 5d, 7d represent the Grad-CAM and the attention maps of the clean(top) and AEs imgs, respectively. It is clear that ViTs have the capability to track the global features of the input image while CNNs track local and centered features. Figures 5a and 7a represent the perturbations of the generated AEs

6. Some image quality assessment methods assume that there is a distortion level at which the distortions start be visible to the observers. When there is a distortion in an image and is not perceptible, it is called near threshold distortion. When the distortion is visible with high magnitude in the image, it is called suprathreshold distortion.
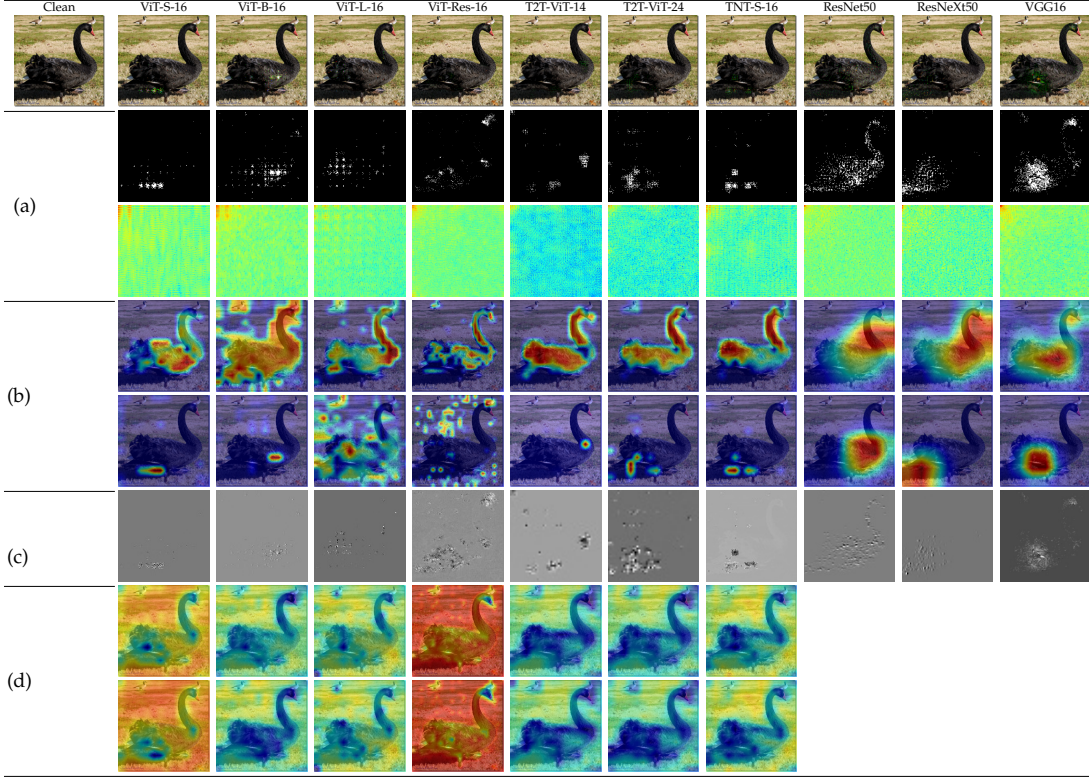
Fig. 5: **JSMA attack:** The first row shows the clean sample and the AEs. The clean image is correctly classified by tested models and all AEs are successful attacks. (a) The perturbation (top) and the corresponding DCT-based spectral decomposition heatmap. Perturbation is shown in black and white colors only. (b) Grad-CAM of the clean (top) and AE samples. (c) Feature map difference between clean and AE feature maps that are computed after the first basic block of the model, attention block for ViTs and convolutional layer for CNNs. (d) The attention map from last attention block for clean (top) and AE samples.
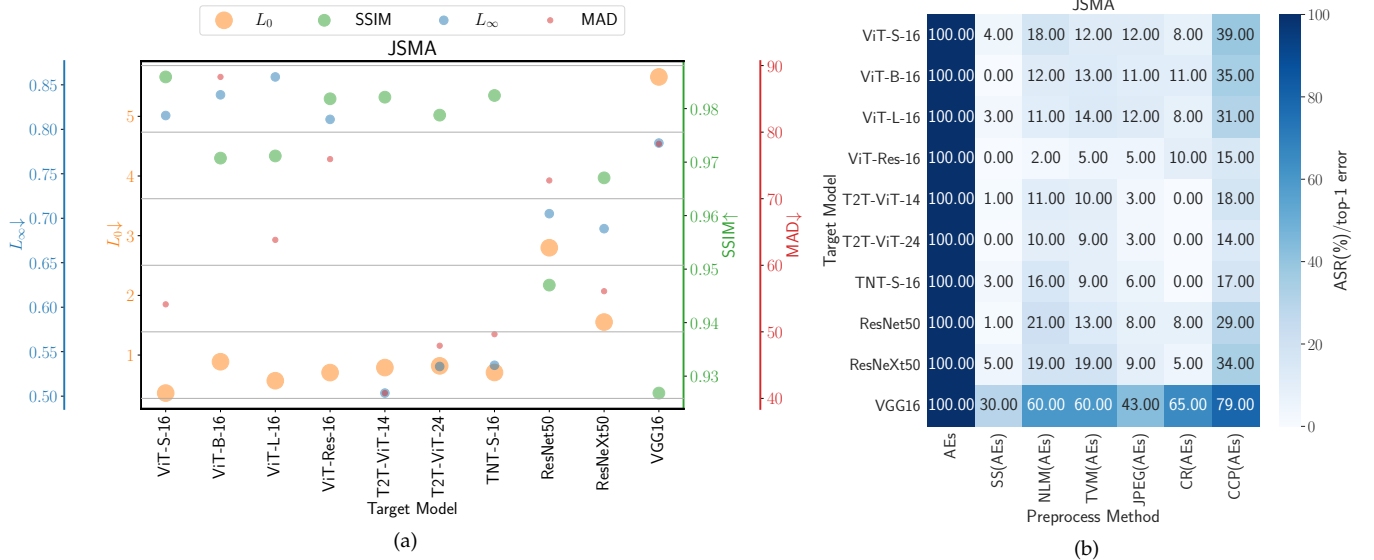

Fig. 6: **JSMA attack:** (a) AEs quality assessment measures. (b) The ASR of the AEs and the top-1 error of the pre-processed AEs on 100 images from imagenet-1k. SS: local spatial smoothing. NLM: non-local mean. TVM: total variation minimization. JPEG: JPEG compression. CR: cropping and re-scaling. CCP: color channel perturbations.

for each model. It is clear that the perturbations highly target the main object of the image, the goose or the dog for both CNNs and vanilla ViTs. Moreover, the effect of the perturbation can be noticed on the Grad-CAM. The impacted regions of the attention and Grad-CAM maps span to regions that are not related to the main object of the image. On the other hand, model's feature maps were known to be affected by the perturbations and propagate when the model goes deeper. As shown in [2], CNNs and hybrid-ViTs tend to better learn low-level features. Figures 5c, and 7c show the difference of clean and AE feature maps after the first convolutional layer for CNNs and after the first attention block for ViTs. As feature maps show, the perturbation impacted learned features, especially the low-level features.

4.2 Vanilla ViTs are more robust against L_0-based attacks

L_0-based attacks rely on changing few image pixels in order to fool the neural networks. Finding these few pixels is challenging and computationally consuming process since the attack algorithms need to search over the image space to identify these pixels. In this work we consider the white-box JSMA attack [38], and generate 100 AEs from ImageNet-1k validation images and a sample is shown in the first row
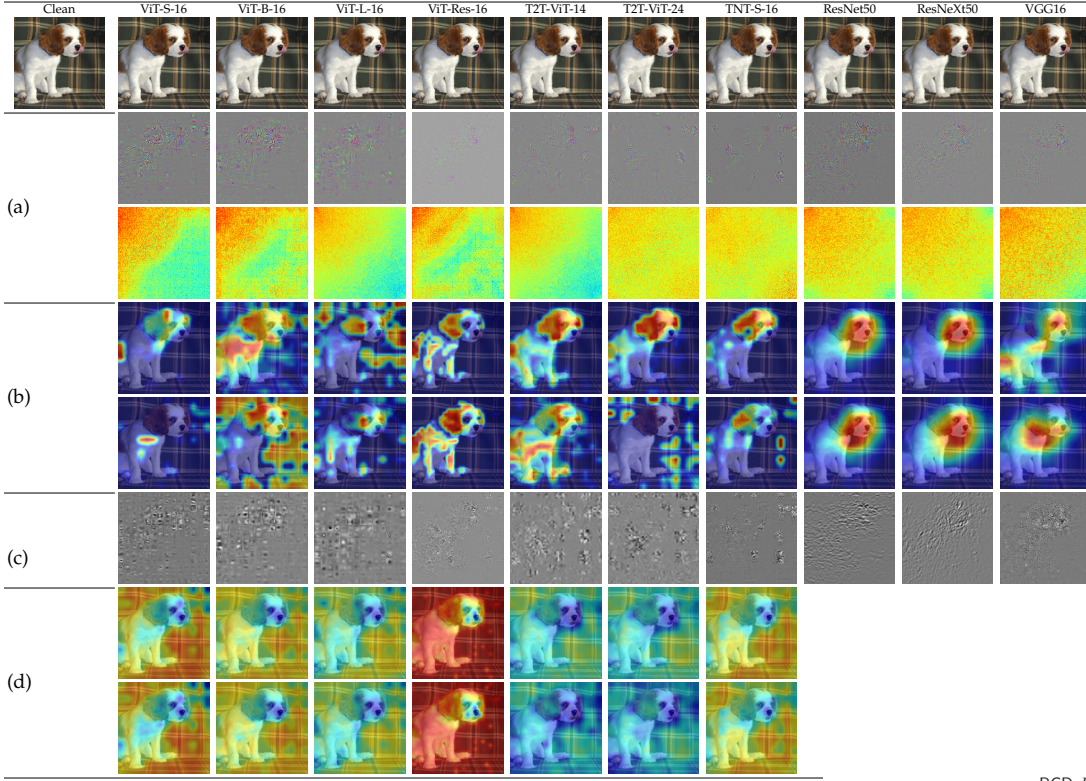
Fig. 7: **PGD-L_1 $\epsilon = 400$ attack:** The first row shows the clean sample and the AEs. The clean image is correctly classified by tested models and all AEs are successful attacks. (a) The perturbation (top) and the corresponding DCT-based spectral decomposition heatmap. Perturbation is scaled from [-1, 1] to [0, 255]. (b) Grad-CAM of the clean (top) and AE samples. (c) Feature map difference between clean and AE feature maps that are computed after the first basic block of the model, attention block for ViTs and convolutional layer for CNNs. (d) The attention map from last attention block for clean (top) and AE samples.
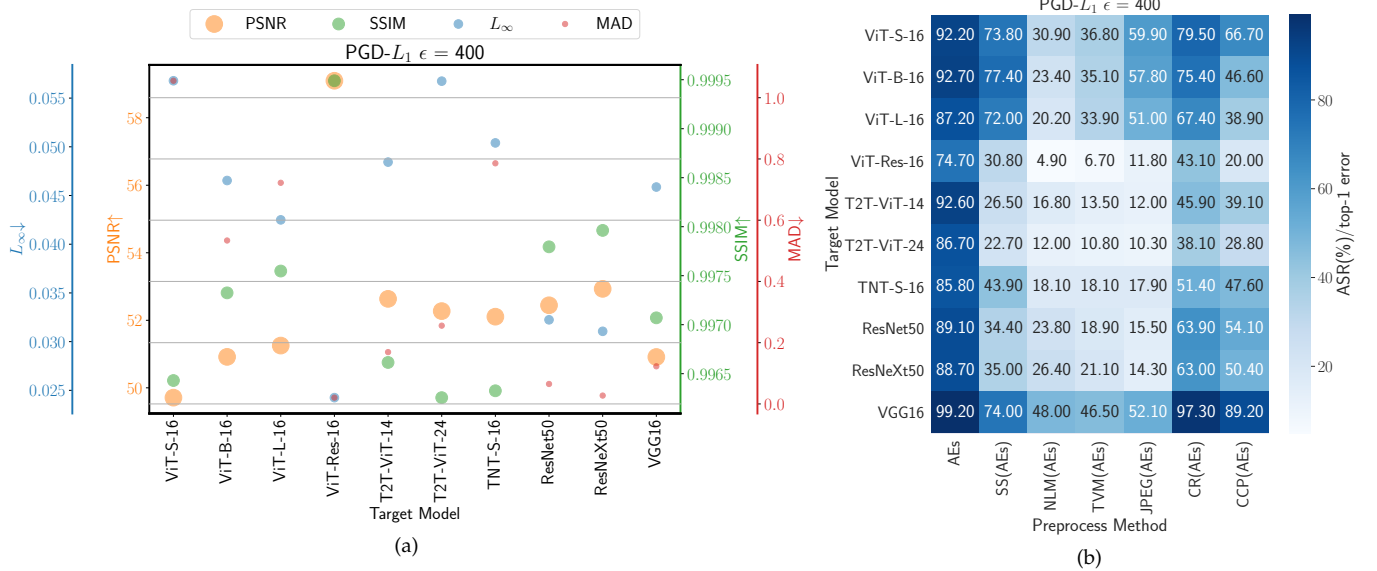

PGD-L_1 $\epsilon = 400$

Target Model	AEs	SS(AEs)	NLM(AEs)	TVM(AEs)	JPEG(AEs)	CR(AEs)	CCP(AEs)
ViT-S-16	92.20	73.80	30.90	36.80	59.90	79.50	66.70
ViT-B-16	92.70	77.40	23.40	35.10	57.80	75.40	46.60
ViT-L-16	87.20	72.00	20.20	33.90	51.00	67.40	38.90
ViT-Res-16	74.70	30.80	4.90	6.70	11.80	43.10	20.00
T2T-ViT-14	92.60	26.50	16.80	13.50	12.00	45.90	39.10
T2T-ViT-24	86.70	22.70	12.00	10.80	10.30	38.10	28.80
TNT-S-16	85.80	43.90	18.10	18.10	17.90	51.40	47.60
ResNet50	89.10	34.40	23.80	18.90	15.50	63.90	54.10
ResNeXt50	88.70	35.00	26.40	21.10	14.30	63.00	50.40
VGG16	99.20	74.00	48.00	46.50	52.10	97.30	89.20

(a)

(b)

Fig. 8: **PGD-L_1 $\epsilon = 400$ attack:** (a) AEs quality assessment measures. (b) The ASR of the AEs and the top-1 error of the pre-processed AEs on 1000 images from ImageNet-1k. SS: local spatial smoothing. NLM: non-local mean. TVM: total variation minimization. JPEG: JPEG compression. CR: cropping and re-scaling. CCP: color channel perturbations.

of Figure 5. The results are investigated and the following observations are noted.

JSMA identifies input features that significantly impact the classification output. In this experiment, JSMA achieves 100% ASR for all tested models, see the first column of Figure 6b. Hence, to study the robustness of a model against L_0-based attacks, we analyzed 1) the perturbation DCT-based spectral decomposition [53], see Figure 5a, that shows that ViTs have a wider spread energy spectrum which confirms a) ViTs are less sensitive to low-level features and exploit the global context of the image, and b) wider frequency spectrum has to be affected to generate AE for ViT models and its variants, 2) the visual quality measures of AEs in Figure 6a show that JSMA, for vanilla ViTs, targeted less

than 1% of the pixels (L_0) and has to increase the densities (L_∞) of the input pixels to more than 0.8, in order to fool the models, which makes vanilla ViTs more robust against L_0-based attacks than hybrid-ViTs.

On the other hand, in CNN, a higher number of pixels are targeted with a high change in pixels intensities, which clearly affect the structure of the AE as SSIM metric clearly shows. While, in hybrid-ViT models, less number of pixels with low pixel intensity change is enough to generate an AE with high quality relative to human perception as MAD measure shows. Moreover, a narrower spread of spectrum energy has been noticed on the DCT-based decomposition, hence, bringing convolutional layers into ViTs doesn't increase robustness under the L_0-based attacks.
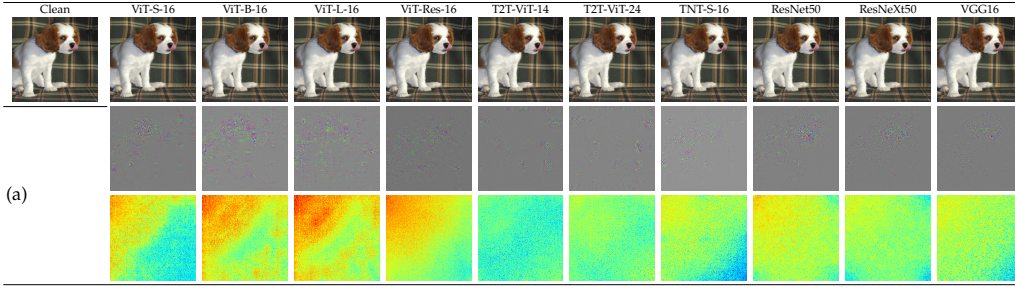
Fig. 9: **CW-L_2 attack:** The first row shows the clean sample and the AEs. The clean image is correctly classified by tested models and all AEs are successful attacks. (a) The perturbation (top) and the corresponding DCT-based spectral decomposition heatmap. Perturbation is scaled from [-1, 1] to [0, 255].
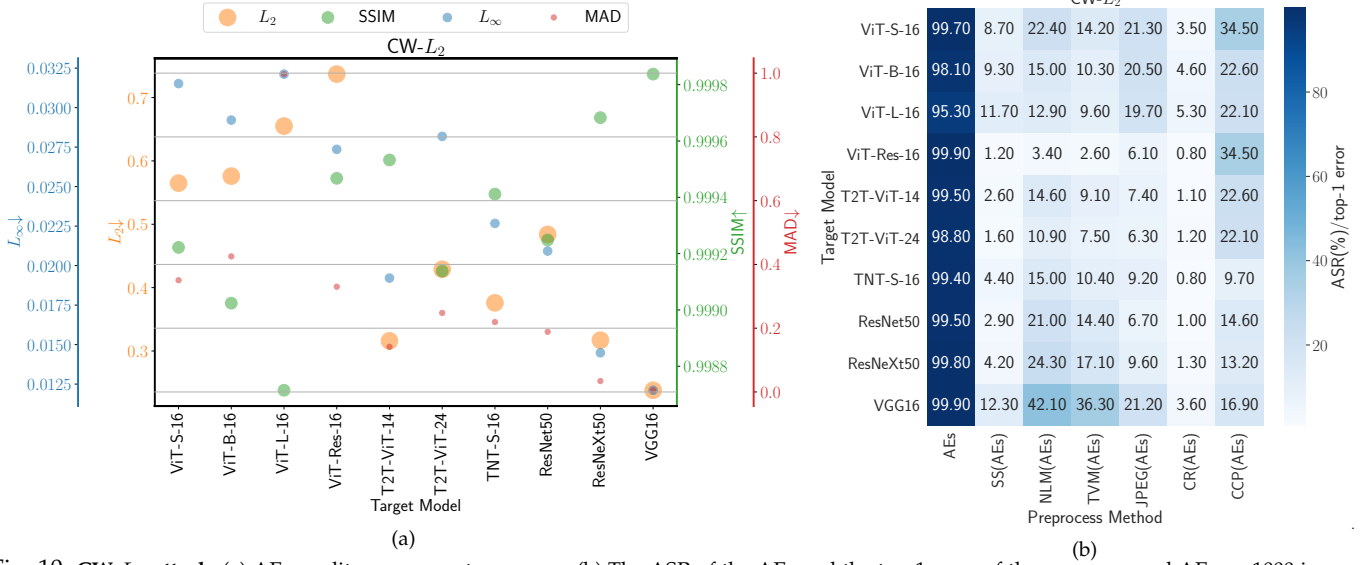

(a)

Target Model	AEs	SS(AEs)	NLM(AEs)	TVM(AEs)	JPEG(AEs)	CR(AEs)	CCP(AEs)
ViT-S-16	99.70	8.70	22.40	14.20	21.30	3.50	34.50
ViT-B-16	98.10	9.30	15.00	10.30	20.50	4.60	22.60
ViT-L-16	95.30	11.70	12.90	9.60	19.70	5.30	22.10
ViT-Res-16	99.90	1.20	3.40	2.60	6.10	0.80	34.50
T2T-ViT-14	99.50	2.60	14.60	9.10	7.40	1.10	22.60
T2T-ViT-24	98.80	1.60	10.90	7.50	6.30	1.20	22.10
TNT-S-16	99.40	4.40	15.00	10.40	9.20	0.80	9.70
ResNet50	99.50	2.90	21.00	14.40	6.70	1.00	14.60
ResNeXt50	99.80	4.20	24.30	17.10	9.60	1.30	13.20
VGG16	99.90	12.30	42.10	36.30	21.20	3.60	16.90

(b)

Fig. 10: **CW-L_2 attack:** (a) AEs quality assessment measures. (b) The ASR of the AEs and the top-1 error of the pre-processed AEs on 1000 images from ImageNet-1k. SS: local spatial smoothing. NLM: non-local mean. TVM: total variation minimization. JPEG: JPEG compression. CR: cropping and re-scaling. CCP: color channel perturbations.

4.3 T2T-ViT-24 and TNT-S-16 are more robust against L_1-based attacks

L_1-based attacks minimize the perturbation δ, where $\delta = ||x - x'||_1$, $\delta \leq \epsilon$, and $f(x) \neq f(x')$, where $f(.)$ is a prediction function. In this work we consider the white-box PGD-L_1 attack [27], and generate 1000 AEs from ImageNet-1k validation images and a sample is shown in the first row of Figure 7. In this experiment, we set ϵ to 400. As shown in the first column of Figure 8b, PGD-L_1 achieves less ASR on ViT-L-16, T2T-ViT-24 and TNT-S-16 models. As shown in Figure 7a, perturbations that are generated using T2T-ViT-24 and TNT-S-16 models have wider frequency spectrum spread than ViT-Res-16 and ViT-L-16 models, which makes them more robust than other models. While perturbations that are generated using ResNets have a wider spread of frequency spectrum than ViT-S/B-16 and T2T-ViT-14. From the visual quality assessment point of view, see Figure 8a, 1) as SSIM scores show, perturbations that are generated using T2T-ViT-24 and TNT-S-16 models have more influence to alter the adversarial image structure than the structure of AEs generated by other models, 2) as PSNR and MAD scores show, perturbations that are generated using ViT variants, in general and specifically T2T-ViT-24 and TNT-S-16, have higher L_∞ than other tested models which yields to have lower image quality of AE. VGG16 has the highest ASR which makes it less robust than other models. One reason for that is that VGG16 has less accuracy performance than other models which makes the learned features not robust.

In this experiment, ViT-Res-16 is excluded from the analysis since the image size is different.

4.4 Vanilla ViTs are more robust under CW-L_2, while hybrid-ViTs are more robust under PGD-L_2 attacks

L_2-based attacks minimize the perturbation δ, where $\delta = ||x - x'||_2$, $\delta \leq \epsilon$, and $f(x) \neq f(x')$. In this work we consider the white-box CW-L_2 [31] and PGD-L_2 attacks [27], and generate 1000 AEs from ImageNet-1k validation images and a sample is shown in the first row of Figure 9.

4.4.1 Robustness under CW-L_2 attacks

As shown in the the first column of Figure 10b, CW-L_2 attack achieves comparable ASR on all tested models except for ViT-L-16 which achieves less ASR. Compared to ResNet, the DCT decomposition of the perturbation shows the huge wide spread of energy spectrum for vanilla ViTs, especially ViT-L-16. Moreover, the algorithm of CW-L_2 has to increase L_2 and L_∞ distortions, see Figure 10a, for ViTs in order to generate successful attacks. Hence, SSIM and MAD show less quality score for AEs that are generated using vanilla ViTs. ResNet shows robustness over T2T-ViT-14 since the perturbations that are generated using ResNet have a wider spread of frequency spectrum than T2T-ViT-14 but not wider than T2T-ViT-24 and TNT-S-16. The visual quality scores, given in Figure 10a, confirm that ResNet is more robust than T2T-ViT-14 but less robust than T2T-ViT-24 and TNT-S-16.
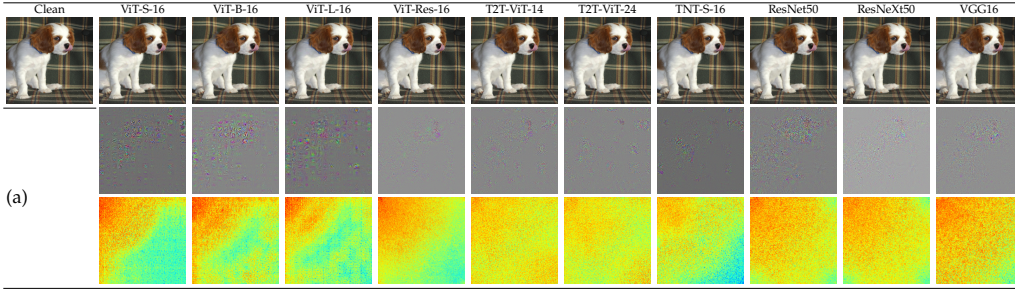
Fig. 11: **PGD-**L_2 $\epsilon = 2$ **attack:** The first row shows the clean sample and the AEs. The clean image is correctly classified by tested models and all AEs are successful attacks. (a) The perturbation (top) and the corresponding DCT-based spectral decomposition heatmap. Perturbation is scaled from [-1, 1] to [0, 255].
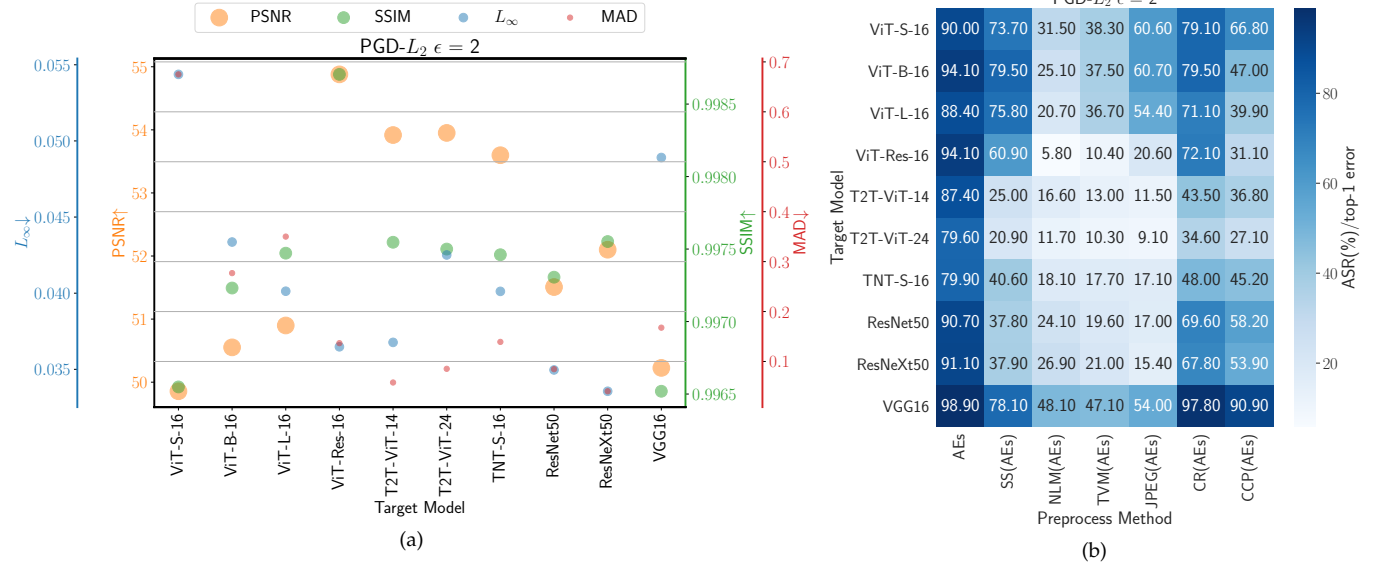

Fig. 12: **PGD-**L_2 $\epsilon = 2$ **attack:** (a) AEs quality assessment measures. (b) The ASR of the AEs and the top-1 error of the pre-processed AEs on 1000 images from imagenet-1k. SS: local spatial smoothing. NLM: non-local mean. TVM: total variation minimization. JPEG: JPEG compression. CR: cropping and re-scaling. CCP: color channel perturbations.

4.4.2 Robustness under PGD-L_2 attacks

Figure 11 shows an example to study the target models' robustness against PGD-L_2 attack with $\epsilon = 2$. From the first column of Figure 12b, we concluded that the hybrid-ViT are more robust than other models against PGD-L_2 attacks. The ASR of the hybrid-ViTs is less than the ASR of the other target models. Moreover, when we look at Figure 11a, we can see that hybrid-ViTs have a wider spread of discriminative features on all frequencies than other models. Moreover, the ViT-S/B/L-16 models show better robustness over ResNet. When looking at Figure 12a, we can see that ViT variants have higher L_∞ score, especially the ViT-S-16, than ResNet which affects the AE structure and visual quality as SSIM and MAD scores show. VGG16 has the highest ASR and high distortion which makes it less robust. One reason for that is that VGG16 has less accuracy performance than other models which makes the learned features not robust. In this experiment, ViT-Res-16 is excluded from the analysis since the image size is different.

Hence, we can conclude that neither larger model's architecture, like ViT-L, nor bringing convolutional modules for tokenization in ViTs, like TNT, will necessarily enhance the robustness.

4.5 Hybrid-ViTs and small ViT are matters under some L_∞-based attacks.

L_∞-based attacks minimize the perturbation δ, where $\delta = ||x - x'||_\infty, \delta \leq \epsilon$, and $f(x) \neq f(x')$. In this work we consider the white-box FGSM-L_∞ [26], CW-L_∞ [31], PGD-L_∞ [27], and UAP [39] attacks. Moreover, two black box attacks are considered; RayS [41] and SA [40] attacks and the AA-L_∞ [30] hybrid attack is considered as well.

4.5.1 Robustness under PGD-L_∞, AA, and UAP attacks

We generate 1000 AEs from ImageNet-1k validation images and a sample is shown in the first row of Figure 13. PGD-L_∞ attack achieves less ASR on ViT-S-16 than other tested models. While ResNets have comparable robustness to ViT-L-16, T2T-ViT-24, and TNT-S-16, and have better robustness over ViT-B-16, ViT-Res-16, and T2T-ViT-14. The perturbations that are generated using ViT-S-16 have the following properties: 1) more spread of energy spectrum as DCT decomposition shows in Figure 13a , 2) lower visual quality as PSNR, SSIM scores show in Figure 14a, and 3) higher L_1 score. L_1 score for ViT-Res-16 is not considered in the analysis since the image size is different. Similar to L_1-based attack, VGG16 has the highest ASR which makes it less robust. VGG16 has the highest ASR and high distortion which makes it less robust than other target tested models.

Under the AA and UAP attacks, we noticed that ViT-S-16 has better robustness than other target models, as Figure 4
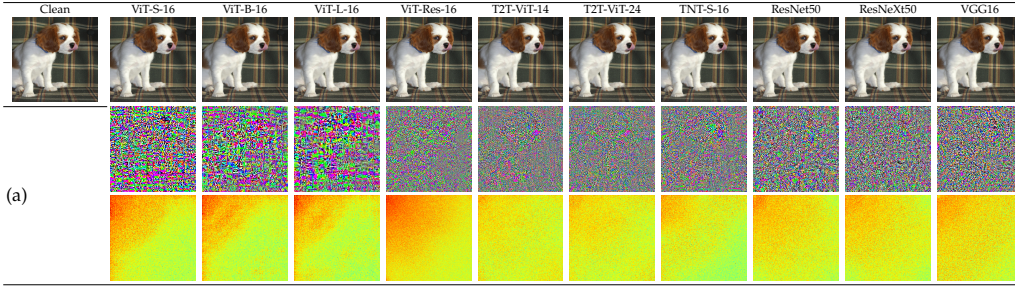
Fig. 13: **PGD-L_∞** $\epsilon = 1/255$ **attack:** First row shows the clean sample and the AEs. The clean image is correctly classified by tested models and all AEs are successful attacks. (a) The perturbation (top) and the corresponding DCT-based spectral decomposition heatmap. Perturbation is scaled from [-1, 1] to [0, 255].
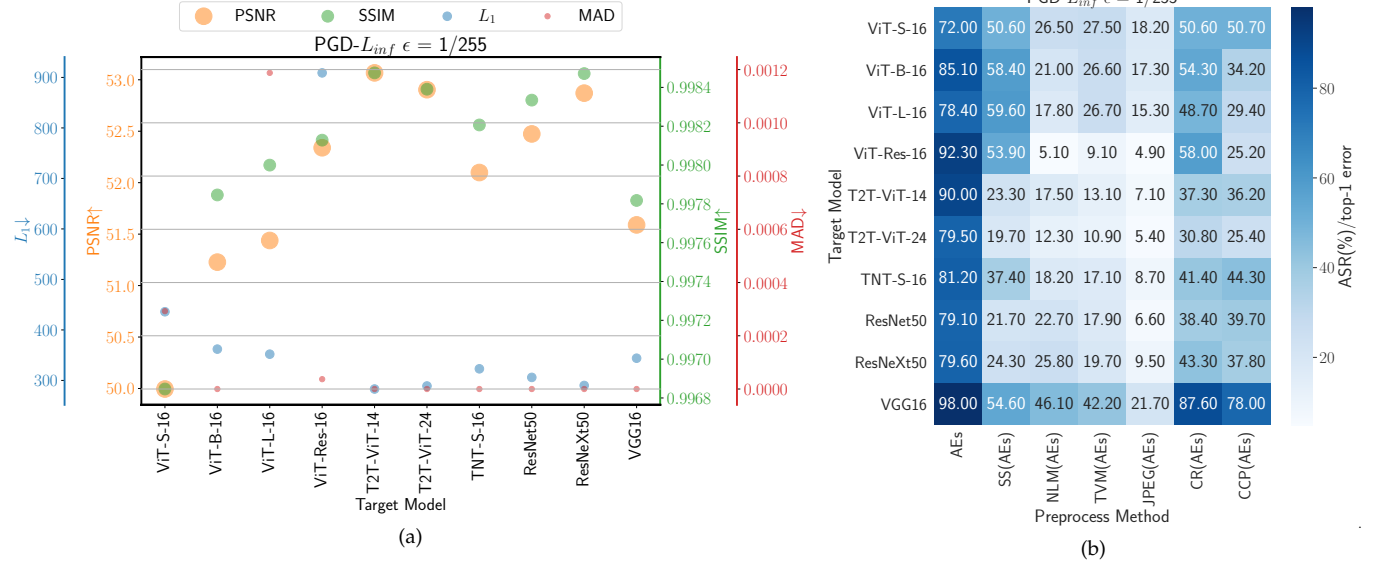

Fig. 14: **PGD-L_∞** $\epsilon = 1/255$ **attack:** (a) AEs quality assessment measures. (b) The ASR of the AEs and the top-1 error of the pre-processed AEs on 1000 images from imagenet-1k. SS: local spatial smoothing. NLM: non-local mean. TVM: total variation minimization. JPEG: JPEG compression. CR: cropping and re-scaling. CCP: color channel perturbations.

shows for AA, but due to space limitation, we only visualized PGD-L_∞ attacks.

4.5.2 Robustness under FGSM-L_∞ attacks

Figure 15 shows an example to study the target models' robustness against FGSM-L_∞ attack. Figure 16a, 18a shows the visual quality scores of the AEs that are generated using FGSM-L_∞ attack. While Figure 16b shows the ASR of the AEs and the top-1 error of the pre-processed AEs that are generated using FGSM-L_∞ attack.

Figure 16b shows that hybrid-ViTs have lower ASR than other models. Vanilla ViT-L-16 shows more robustness over ResNet and ReNeXt, while ResNet shows robustness over vanilla ViT-S/B-16. The wider spread of the energy spectrum of the DCT decomposition confirms the robustness of hybrid-ViTs over other models, as shown in Figure 15a. Moreover, SSIM scores, illustrated in Figure 16a, show that hybrid-ViT has lower score than other models, except for VGG16. VGG16 has the lowest robustness since it has the highest ASR and high distortion as SSIM score indicates. In FGSM attack, it is hard to use PSNR and MAD to judge the robustness of the target models since the $||\delta||_2$ of all generated AEs are equal.

4.5.3 Robustness under CW-L_∞ attacks

Figure 17 shows an example to study the target models' robustness against CW-L_∞ attack. Figure 18a shows the visual quality scores of the AEs that are generated using CW-L_∞ attack. While Figure 18b shows the ASR of the AEs and

the top-1 error of the pre-processed AEs that are generated using CW-L_∞ attack.

For CW-L_∞, Figure 18b shows that the ASR of the ViT-B/L-16 is lower than the ASR of other models. On the other hand, the DCT decomposition, see Figure 17a, shows that the spread of the discriminative features is wider on ViT-B/L-16 than other models. Moreover, it is shown that T2T-ViT-24 and TNT-S-16 have wider spread of DCT decomposition than ResNet. Finally, from Figure 18a, we can conclude that CW-L_∞ generates AEs with higher perturbations for ViT-B/L-16 and for T2T-ViT-24 models than other model which clearly affected the image structure and the visual perception as SSIM and MAD scores indicate.

4.5.4 Robustness under RayS attacks

Figure 19 shows an example to study the target models' robustness against RayS attack. Figure 20a shows the visual quality scores of the AEs that are generated using RayS attack. While Figure 20b shows the ASR of the AEs and the top-1 error of the pre-processed AEs that are generated using RayS attack.

For RayS attack, by looking at Figure 20b, Figure 19a, and Figure 20a, we can conclude that hybrid-ViTs are more robust than other target models. The figures show 1) T2T-ViT-24 has lower ASR than other models. 2) hybrid-ViTs have wider energy spectrum spread than other models. 3) RayS generates AEs with higher perturbations for hybrid-ViTs that are perceptible to human.
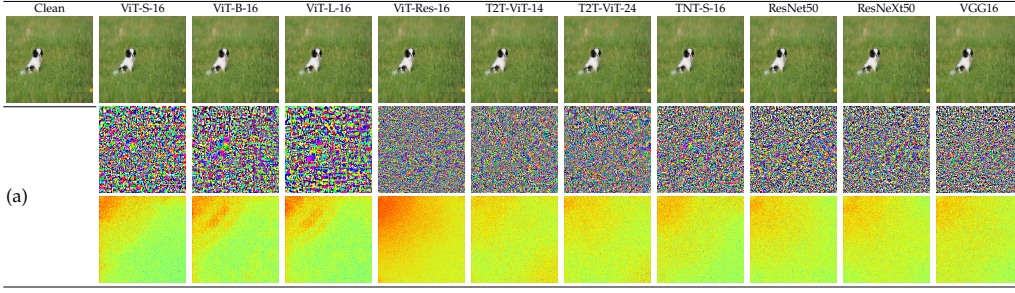
Fig. 15: **FGSM-L_∞ $\epsilon = 1/255$ attack:** The first row shows the clean sample and the AEs. The clean image is correctly classified by tested models and all AEs are successful attacks. (a) The perturbation (top) and the corresponding DCT-based spectral decomposition heatmap. Perturbation is scaled from [-1, 1] to [0, 255].
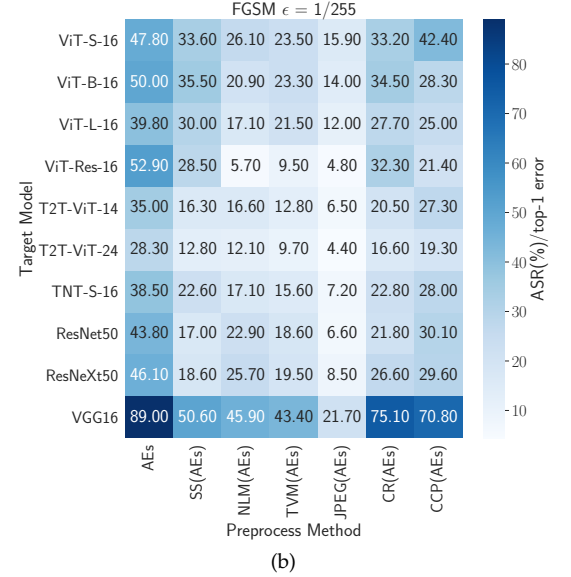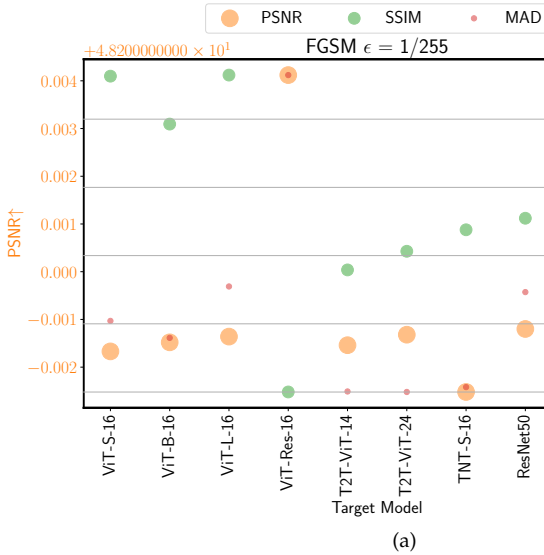

(a)

Target Model	AEs	SS(AEs)	NLM(AEs)	TVM(AEs)	JPEG(AEs)	CR(AEs)	CCP(AEs)
ViT-S-16	47.80	33.60	26.10	23.50	15.90	33.20	42.40
ViT-B-16	50.00	35.50	20.90	23.30	14.00	34.50	28.30
ViT-L-16	39.80	30.00	17.10	21.50	12.00	27.70	25.00
ViT-Res-16	52.90	28.50	5.70	9.50	4.80	32.30	21.40
T2T-ViT-14	35.00	16.30	16.60	12.80	6.50	20.50	27.30
T2T-ViT-24	28.30	12.80	12.10	9.70	4.40	16.60	19.30
TNT-S-16	38.50	22.60	17.10	15.60	7.20	22.80	28.00
ResNet50	43.80	17.00	22.90	18.60	6.60	21.80	30.10
ResNeXt50	46.10	18.60	25.70	19.50	8.50	26.60	29.60
VGG16	89.00	50.60	45.90	43.40	21.70	75.10	70.80

Preprocess Method

(b)

Fig. 16: **FGSM-L_∞ $\epsilon = 1/255$ attack:** (a) AEs quality assessment measures. (b) The ASR of the AEs and the top-1 error of the pre-processed AEs on 1000 images from imagenet-1k. SS: local spatial smoothing. NLM: non-local mean. TVM: total variation minimization. JPEG: JPEG compression. CR: cropping and re-scaling. CCP: color channel perturbations.

4.6 Transfer attacks: increasing the number of attention blocks reduces the transferability

Recent studies in [17], [18], [19] showed that there is low transferability between different models' families. In this work we confirm that and the results are shown in Figure 21a. Here, we show two new observations. The first one is that the transferability, within the same model family, is becoming lower when the model is becoming larger. Hence, adding more attention blocks to ViT variant models reduces the effect of the transferability property, as shown in Figure 21a. The second[7] observation is that the black box based AEs, RayS and SA, that are generated using ViT variants are more transferable to CNNs while the black box based AEs that are generated using CNN are much less transferable to ViT variants. As shown in Figure 21b, we notice that when CNNs serve as target models, last three columns, the ASR is higher than those of when CNNs serve as the source model, last three rows. According to the DCT decomposition of SA-based AEs, see Figure 22, one possible explanation to this case is that the generated perturbations highly affect the local features than global features and since ViTs are less sensitive to local features making perturbation effect less transferable.

---

7. Using source model to generate black box AEs for a different target model is not popular in real-world but, here the goal is to note the observation.

4.7 Color channel perturbations (CCP) is an attack and defense!

The CCP attack is based on the color property of the image. It uses the original color channels, Red R, Green G and Blue B of the image input x to generate the AE (x'). The AE is composed of new transformed color channels, R', G', and B' of the transformed image (x'). The transformed channels are calculated as follows:

$$R' = s\left(\frac{\alpha^r R + \alpha^g G + \alpha^b B}{3}\right) + b,$$

$$G' = s\left(\frac{\beta^r R + \beta^g G + \beta^b B}{3}\right) + b, \quad (5)$$

$$B' = s\left(\frac{\gamma^r R + \gamma^g G + \gamma^b B}{3}\right) + b,$$

where s is a scale factor hyperparameter, b is a bias hyperparameter, $\{\alpha, \beta, \gamma\} \in [0, 1]$, and $\{R', G', B'\} \in \mathbb{R}$. The scale s and bias b are used to adjust the visual appearance of the generated AE. Figure 23 shows examples for CCP attack.

Images might be vulnerable to natural perturbations like color brightness change. Table 3 shows the ASR of the target models against the CCP attack. Although this attack doesn't achieve high ASR when tested on neural network models, it can reveal robustness of these models. The results in Table 3 show that hybrid-ViTs have the highest robustness, while
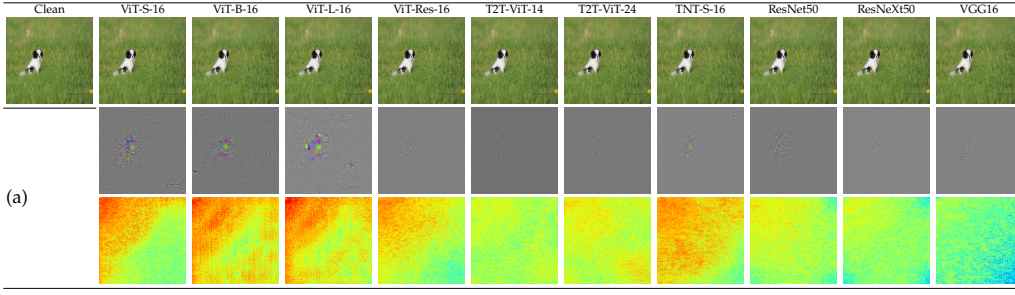
Fig. 17: **CW-L_∞ attack:** The first row shows the clean sample and the AEs. The clean image is correctly classified by tested models and all AEs are successful attacks. (a) The perturbation (top) and the corresponding DCT-based spectral decomposition heatmap. Perturbation is scaled from [-1, 1] to [0, 255].
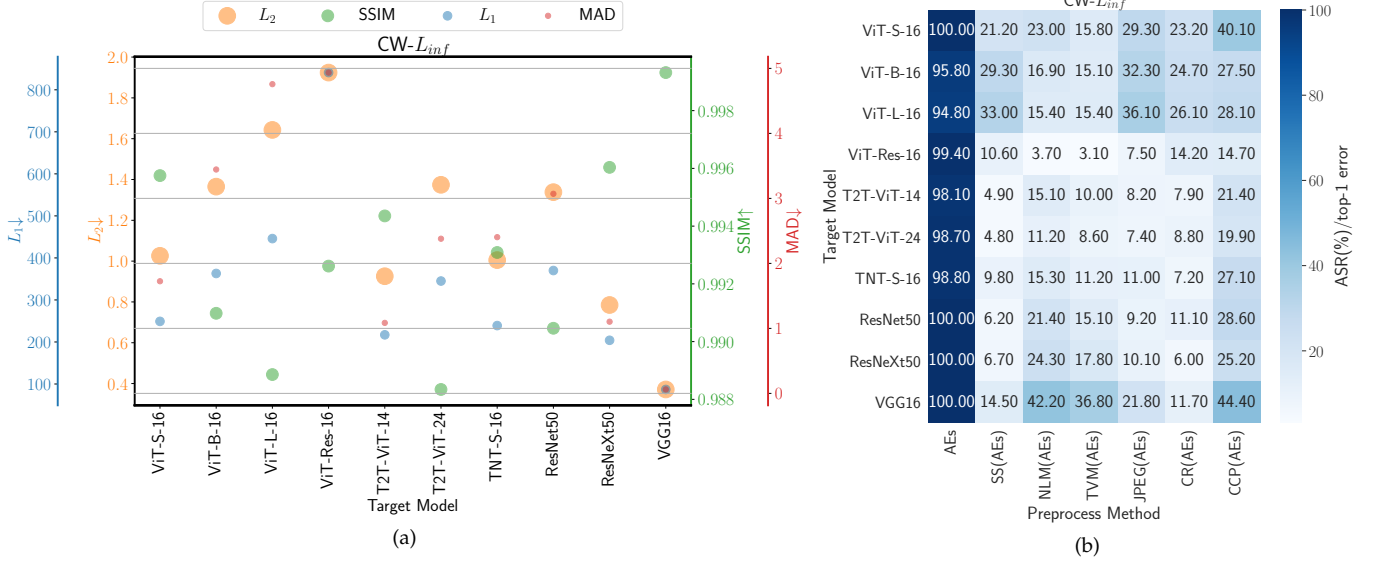

Fig. 18: **CW-L_∞ attack:** (a) AEs quality assessment measures. (b) The ASR of the AEs and the top-1 error of the pre-processed AEs on 1000 images from imagenet-1k. SS: local spatial smoothing. NLM: non-local mean. TVM: total variation minimization. JPEG: JPEG compression. CR: cropping and re-scaling. CCP: color channel perturbations.

Target Model	AEs	SS(AEs)	NLM(AEs)	TVM(AEs)	JPEG(AEs)	CR(AEs)	CCP(AEs)
ViT-S-16	100.00	21.20	23.00	15.80	29.30	23.20	40.10
ViT-B-16	95.80	29.30	16.90	15.10	32.30	24.70	27.50
ViT-L-16	94.80	33.00	15.40	15.40	36.10	26.10	28.10
ViT-Res-16	99.40	10.60	3.70	3.10	7.50	14.20	14.70
T2T-ViT-14	98.10	4.90	15.10	10.00	8.20	7.90	21.40
T2T-ViT-24	98.70	4.80	11.20	8.60	7.40	8.80	19.90
TNT-S-16	98.80	9.80	15.30	11.20	11.00	7.20	27.10
ResNet50	100.00	6.20	21.40	15.10	9.20	11.10	28.60
ResNeXt50	100.00	6.70	24.30	17.80	10.10	6.00	25.20
VGG16	100.00	14.50	42.20	36.80	21.80	11.70	44.40

ResNets and ViT-B/L-16 have comparable robustness. One explanation to that is that CCP limits CNNs' and vanilla ViTs' capabilities to extract the local and global features, respectively. Hence, enhancing the tokenization process of the vanilla ViTs as in hybrid-ViTs has an added value to model's robustness. Surprisingly, we found that when applying CCP attack on AEs, CCP is able to project the AEs back to its original manifold. Last columns of Figures 6b, 8b, 10b, and, 14b show the ASR after considering CCP as a preprocess method for the AEs. Although removing the effect of perturbations depends on noise amount, hybrid-ViTs show better performance on predicting the original class due the presence of the tokenization process enhancements in hybrid-ViTs. Future investigations are highly recommended to study this phenomenon since brightness change is a common process in many real-world applications.

4.8 Vanilla ViTs are not responding to preprocessing defenses that mainly reduce the high frequency components.

Preprocessing is one of the defense methods that is applied to the model's input to remove the effect of perturbations that are added to the input image. In this experiment, we apply five preprocessing methods that are used in the literature and briefly mentioned in Section 3.3. Samples of top-1 error after perprocessing of some attacks are shown in Figures 6b, 8b, 10b, 12b, 14b, 16b, 18b, and 20b, while Figure 1 shows

the top-1 error AA, in average. For L_0-based and CW-L_2 attacks, SS and cropping and re-scaling (CR), as expected, have the capability to remove the perturbations effect and to project AEs back to input manifold, see Figure 6b, by repositioning the perturbation structure. The limited success of the preprocessing against L_0-based AEs that are generated using VGG16 is due the large number of the impacted pixels. For other attacks, NLM and total variation minimization (TVM) show better performance on the preprocessing of AEs. That's because these two denoising methods try to restore the original image while preserving the global image structure and contours. While other preprocessing methods including SS, JPEG, and CR, are highly impacting the high frequency components of the AEs, hence ResNets show better top-1 error over vanilla ViTs. Hybrid-ViTs have lower top-1 error than vanilla ViTs and CNNs due to its power of identifying global and local features. Figure 24 shows examples of the preprocessing process for PGD-L_∞ attacks.

4.9 Robustness under EOT attack

EOT is a framework that constructs AEs that remain adversarial over a chosen transformation distribution T, i.e. the preprocessing defenses. When processing defenses are used the stochastic gradients issue of the classifier $f(.)$ arises and hence, to have successful attack, it is necessary to estimate the gradient over the expected transformation to the input $t(x)$, where, $t(.)$ is the transformation function. EOT optimizes the

TABLE 3: The ASR of the target models against color channel perturbations (CCP).

	ViT-S-16	ViT-B-16	ViT-L-16	ViT-Res-16	T2T-ViT-14	T2T-ViT-24	TNT-S-16	ResNet50	ResNeXt50	VGG16
ASR(%)	22.6	15.2	12.5	**5.4**	**10.1**	**7.1**	**8.1**	11.9	14.9	32.6

TABLE 4: The top-1 error(%) of the preprocessing defense methods that are applied to PGD-L_∞ $\epsilon = 4/255$ under the EOT. 1000 images from imagenet-1k are used. SS: local spatial smoothing. NLM: non-local mean. TVM: total variation minimization. JPEG: JPEG compression. CR: cropping and re-scaling. EOT: expectation over transformation.

Model	No defense	SS		NLM		TVM		JPEG		CR	
EOT	✗	✗	✓	✗	✓	✗	✓	✗	✓	✗	✓
ViT-S-16	99.9	96.3	98	43.8	77.7	62	91.2	91.8	94.3	97.4	90.3
ViT-B-16	99.5	97.2	97.9	35.9	86.4	58.5	94.4	90.2	94.8	96.4	95.6
ViT-L-16	98.8	96.5	97	33.2	83.9	58.6	91.6	88.2	94	93.7	92
ViT-Res-16	100	96.7	99.6	12.3	89.6	34.1	97.8	57.5	96.9	98.1	98.2
T2T-ViT-14	99.9	58.1	96.8	22.8	77.1	24.3	87.4	25	77.4	74.7	70
T2T-ViT-24	99.6	52.3	94.6	18.1	66	21.2	82.1	23.9	70.1	67.4	63.8
TNT-S-16	99.7	80.7	97.8	27.1	78.8	34.2	91.1	38.4	82.2	83	79.7
ResNet50	98.7	61.4	95.7	26.9	81.3	26.3	89	27.9	85.4	86.8	79.4
ResNet50-32x4d	98.4	56.3	95	29.4	79.8	25.4	87.2	22.5	79.3	81.8	71.9
VGG16	99.6	94.1	96.5	55	89.2	57.7	90.2	73.8	95.5	99.4	94.5

expectation over the transformation $_{t\sim T} f(t(x))$ which can be solved by minimizing the expected perceived distance as seen by the classifier $\mathbb{E}_{t\sim T}[d(t(x'), t(x))]$, where $d(.)$ is the distance function.

We consider the distribution of transformations that includes SS, NLM, TVM, JPEG, and CR. We 1) use 1000 images from the ImageNet-1k validation set, 2) generate AEs using PGDs-L_∞ $\epsilon = 4/255$ and apply the preprocessing defense methods for the generated AEs, 3) use EOT to synthesize AEs that are robust over the given distribution T and apply the preprocessing defense methods for the synthesized AEs. Table 4 shows the top-1 error for the target models against the preprocessed AEs with and without considering the EOT.

It is clear that the EOT kept the input samples as adversarial over the tested transformations except for the cropping and re-scaling (CR) transformation. For SS and JPEG , the top-1 error is highly increased in T2T-ViT and ResNets models and the T2T-ViT models show less top-1 error. While for NLM, the small ViT, T2T-ViT, and TNT models have less top-1 error compared to other models. It is interesting to notice that, with the use EOT, the ResNet models have less top-1 error than ViT-B/L models. One reason for that is that the transformation under the EOT highly impacts the global structure of the input sample. For TVM, the top-1 error of T2T-ViT models is less than other target models. The top-1 error for using CR under the EOT is comparable to the top-1 error without CR. One reason for that is that CR, under any framework, targets restructuring the adversarial sample by re-positioning the input pixels.

In general, we conclude that T2T-ViT and TNT models show better robustness than vanilla ViTs and ResNets under the EOT robustness test.

5 CONCLUSION

In this paper, we have studied the robustness of vision transformers and their variants and compared them with

CNNs. Our analysis showed 1) either vanilla ViTs or hybrid-ViTs are more robust than CNNs against L_p-based attacks and CCP attacks. We analysed the energy spectrum of DCT decomposition of the perturbations and the different visual quality measures. 2) CCP can be used as a preprocessing defense method. 3) Increasing the number of attention blocks will increase the robustness against the transfer attacks but not against white box attacks. 4) Enhancing ViT tokenization might not increase the robustness against the AEs but will increase the robustness under the preprocessed AEs.

REFERENCES

[1] K. He, X. Zhang, S. Ren, and J. Sun, "Deep residual learning for image recognition," in *Proceedings of the IEEE conference on computer vision and pattern recognition*, 2016, pp. 770–778. 1, 4

[2] L. Yuan, Y. Chen, T. Wang, W. Yu, Y. Shi, F. E. H. Tay, J. Feng, and S. Yan, "Tokens-to-Token ViT: Training vision transformers from scratch on imagenet," *CoRR*, vol. abs/2101.11986, 2021. 1, 2, 3, 4, 5, 7

[3] A. Vaswani, N. Shazeer, N. Parmar, J. Uszkoreit, L. Jones, A. N. Gomez, L. Kaiser, and I. Polosukhin, "Attention is all you need," in *Advances in Neural Information Processing Systems 30, December 4-9, 2017, Long Beach, CA, USA*, 2017, pp. 5998–6008. 1

[4] A. Dosovitskiy, L. Beyer, A. Kolesnikov, D. Weissenborn, X. Zhai, T. Unterthiner, M. Dehghani, M. Minderer, G. Heigold, S. Gelly, J. Uszkoreit, and N. Houlsby, "An image is worth 16x16 words: Transformers for image recognition at scale," in *9th International Conference on Learning Representations, ICLR 2021, Virtual Event, Austria, May 3-7, 2021*. OpenReview.net, 2021. 1, 3, 4, 5

[5] C. Sun, A. Shrivastava, S. Singh, and A. Gupta, "Revisiting unreasonable effectiveness of data in deep learning era," in *IEEE International Conference on Computer Vision, ICCV 2017, Venice, Italy, October 22-29, 2017*. IEEE Computer Society, 2017, pp. 843–852. 1, 2

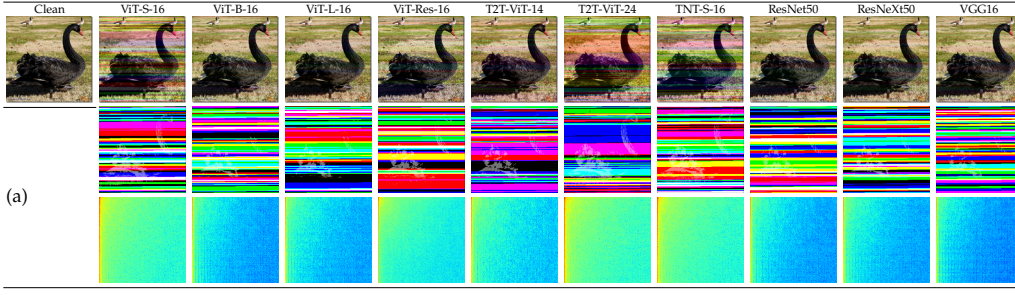[6] J. Deng, W. Dong, R. Socher, L.-J. Li, K. Li, and L. Fei-Fei, in *CVPR09*, 2009. 1, 2, 3, 4

Fig. 19: **RayS attack:** The first row shows the clean sample and the AEs. The clean image is correctly classified by tested models and all AEs are successful attacks. (a) The perturbation (top) and the corresponding DCT-based spectral decomposition heatmap. Perturbation is scaled from [-1, 1] to [0, 255].
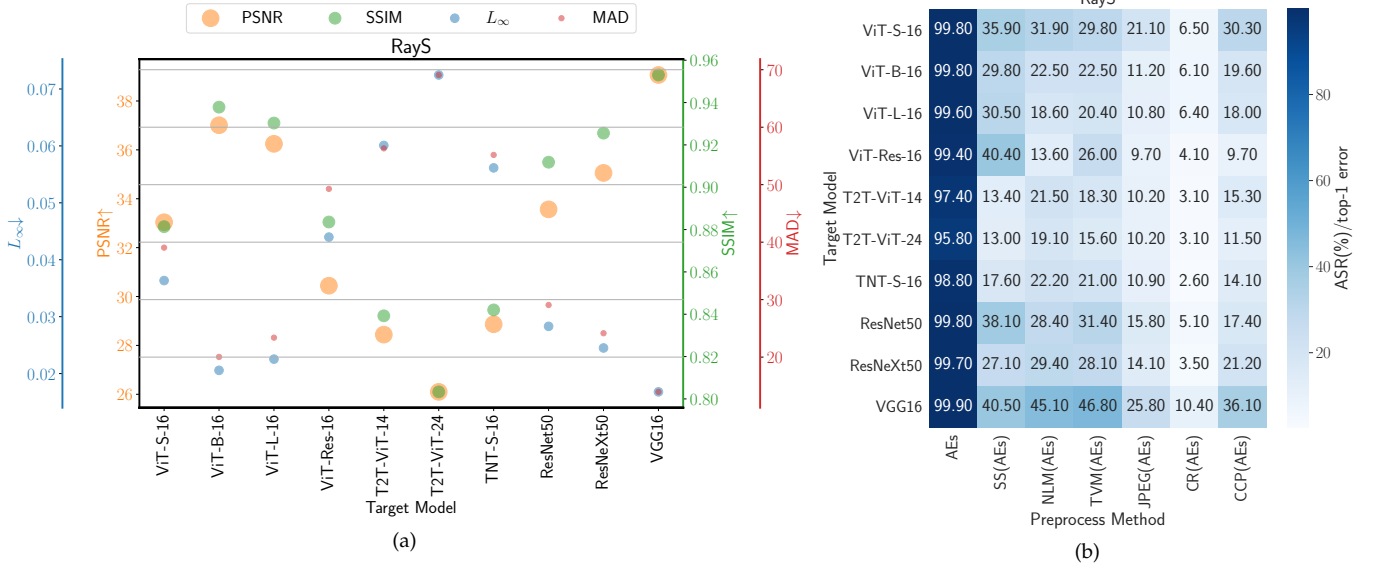

(a)

(b)

Fig. 20: **RayS attack:** (a) AEs quality assessment measures. (b) The ASR of the AEs and the top-1 error of the pre-processed AEs on 1000 images from imagenet-1k. SS: local spatial smoothing. NLM: non-local mean. TVM: total variation minimization. JPEG: JPEG compression. CR: cropping and re-scaling. CCP: color channel perturbations.
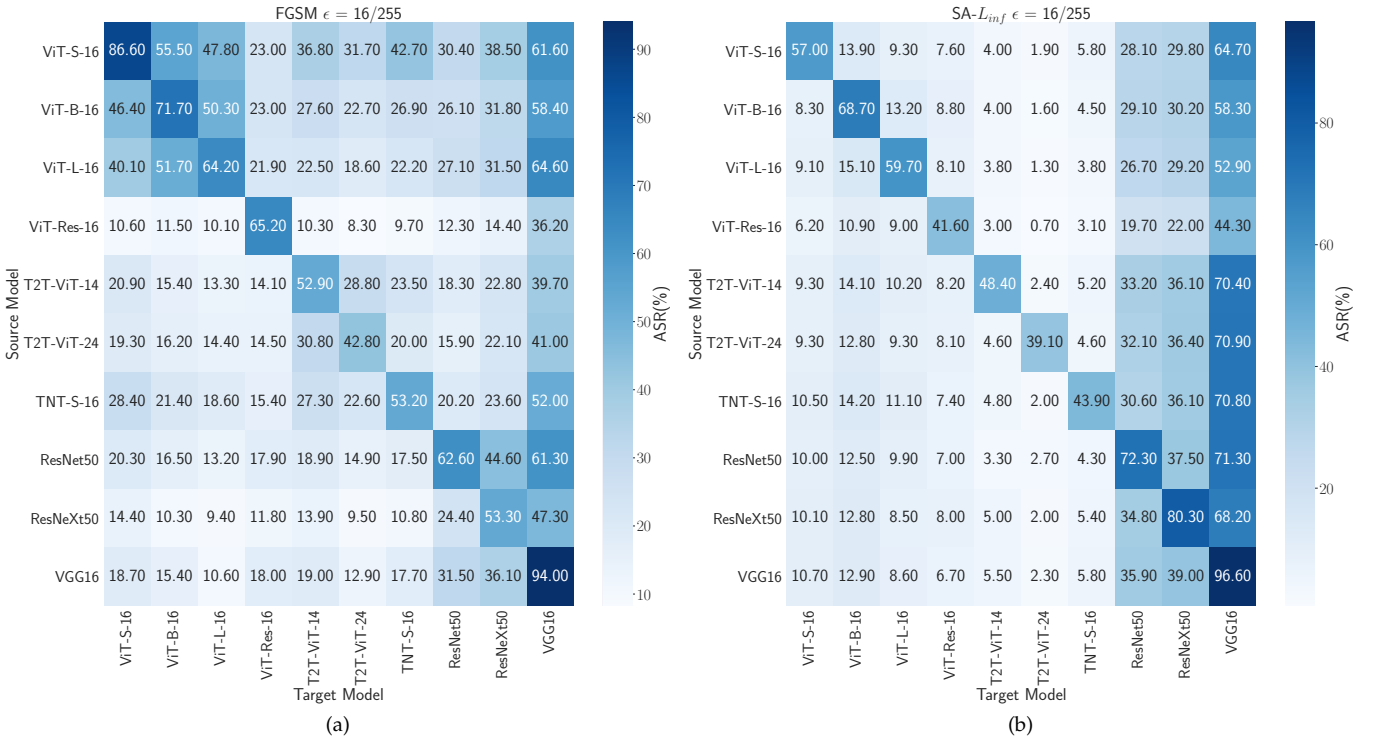

(a)

(b)

Fig. 21: ASR of transfer attack using FGSM and SA on 1000 images from ImageNet-1k . The row represents the source model that is used to generate AE. The column represents the target model. Dark blue column means that the target model is vulnerable to transfer attacks.
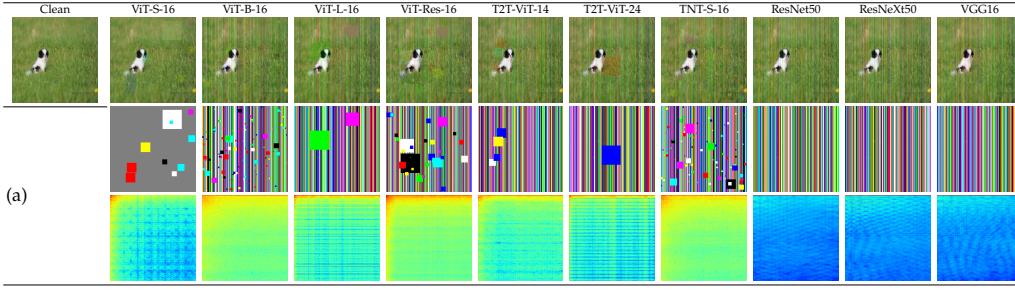
Fig. 22: **SA-**L_∞ $\epsilon = 8/255$ **attack:** The first row shows the clean sample and the AEs. The clean image is correctly classified by tested models and all AEs are successful attacks. (a) The perturbation (top) and the corresponding DCT-based spectral decomposition heatmap. Perturbation is scaled from [-1, 1] to [0, 255].

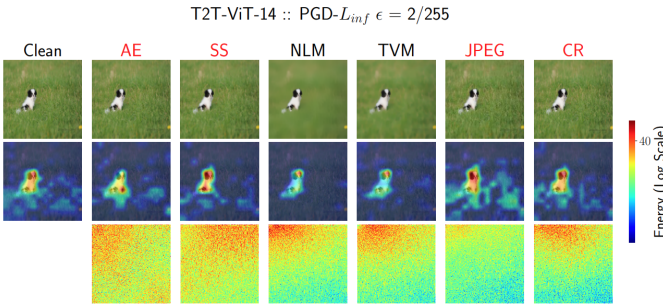Fig. 23: Examples for CCP attack. Images are from ImageNet-1k validation set.

Fig. 24: Examples of the defense preprocessing. The top row shows the clean, AE, and the preprocessed AE. The middle row shows the Grad-CAM of the clean, AE, and the preprocessed AE. The bottom row shows the energy spectrum of the DCT decomposition of AE, and the preprocessed AE. Red label means the image is misclassified.

[7] K. Han, A. Xiao, E. Wu, J. Guo, C. Xu, and Y. Wang, "Transformer in transformer," *CoRR*, vol. abs/2103.00112, 2021. 1, 3, 4

[8] H. Wu, B. Xiao, N. Codella, M. Liu, X. Dai, L. Yuan, and L. Zhang, "CvT: Introducing convolutions to vision transformers," *CoRR*, vol. abs/2103.15808, 2021. 1

[9] K. Simonyan and A. Zisserman, "Very deep convolutional networks for large-scale image recognition," in *3rd International Conference on Learning Representations, ICLR 2015, San Diego, CA, USA, May 7-9, 2015, Conference Track Proceedings*, Y. Bengio and Y. LeCun, Eds., 2015. 1, 4

[10] C. Szegedy, V. Vanhoucke, S. Ioffe, J. Shlens, and Z. Wojna, "Rethinking the inception architecture for computer vision," in *Proceedings of the IEEE conference on computer vision and pattern recognition*, 2016, pp. 2818–2826. 1

[11] A. G. Howard, M. Zhu, B. Chen, D. Kalenichenko, W. Wang, T. Weyand, M. Andreetto, and H. Adam, "MobileNets: Efficient convolutional neural networks for mobile vision applications," *arXiv preprint arXiv:1704.04861*, 2017. 1

[12] C. Szegedy, W. Zaremba, I. Sutskever, J. Bruna, D. Erhan, I. J. Goodfellow, and R. Fergus, "Intriguing properties of neural networks," in *2nd International Conference on Learning Representations, ICLR 2014, Banff, AB, Canada, April 14-16, 2014, Conference Track Proceedings*, 2014. 1, 2

[13] N. Carlini and D. Wagner, "Adversarial examples are not easily detected: Bypassing ten detection methods," in *Proceedings of the 10th ACM Workshop on Artificial Intelligence and Security*, 2017, pp. 3–14. 1

[14] A. Ilyas, S. Santurkar, D. Tsipras, L. Engstrom, B. Tran, and A. Madry, "Adversarial examples are not bugs, they are features," in *Advances in Neural Information Processing Systems*, 2019, pp. 125–136. 1

[15] N. Akhtar and A. Mian, "Threat of adversarial attacks on deep learning in computer vision: A survey," *IEEE Access*, vol. 6, pp. 14 410–14 430, 2018. 1, 2

[16] H. X. Y. M. Hao-Chen, L. D. Deb, H. L. J.-L. T. Anil, and K. Jain, "Adversarial attacks and defenses in images, graphs and text: A review," *International Journal of Automation and Computing*, vol. 17, no. 2, pp. 151–178, 2020. 1, 2

[17] S. Bhojanapalli, A. Chakrabarti, D. Glasner, D. Li, T. Unterthiner, and A. Veit, "Understanding robustness of transformers for image classification," *CoRR*, vol. abs/2103.14586, 2021. 1, 2, 12

[18] R. Shao, Z. Shi, J. Yi, P. Chen, and C. Hsieh, "On the adversarial robustness of visual transformers," *CoRR*, vol. abs/2103.15670, 2021. 1, 2, 3, 4, 12

[19] K. Mahmood, R. Mahmood, and M. van Dijk, "On the robustness of vision transformers to adversarial examples," 2021. 1, 2, 12

[20] S. Paul and P. Chen, "Vision transformers are robust learners," *CoRR*, vol. abs/2105.07581, 2021. 1, 2

[21] X. Yuan, P. He, Q. Zhu, and X. Li, "Adversarial examples: Attacks and defenses for deep learning," *IEEE transactions on neural networks and learning systems*, vol. 30, no. 9, pp. 2805–2824, 2019. 2

[22] A. Chakraborty, M. Alam, V. Dey, A. Chattopadhyay, and D. Mukhopadhyay, "Adversarial attacks and defences: A survey," *CoRR*, vol. abs/1810.00069, 2018. 2

[23] A. Aldahdooh, W. Hamidouche, S. A. Fezza, and O. Déforges, "Adversarial example detection for DNN models: A review," *CoRR*, vol. abs/2105.00203, 2021. 2

[24] F. Alamri, S. Kalkan, and N. Pugeault, "Transformer-encoder detector module: Using context to improve robustness to adversarial attacks on object detection," in *2020 25th International Conference on Pattern Recognition (ICPR)*. IEEE, 2021, pp. 9577–9584. 2

[25] S. Ren, K. He, R. B. Girshick, and J. Sun, "Faster R-CNN: towards real-time object detection with region proposal networks," *IEEE Trans. Pattern Anal. Mach. Intell.*, vol. 39, no. 6, pp. 1137–1149, 2017. 2

[26] I. J. Goodfellow, J. Shlens, and C. Szegedy, "Explaining and harnessing adversarial examples," in *3rd International Conference on Learning Representations, ICLR 2015, San Diego, CA, USA, May 7-9, 2015, Conference Track Proceedings*, 2015. 2, 4, 10

[27] A. Madry, A. Makelov, L. Schmidt, D. Tsipras, and A. Vladu, "Towards deep learning models resistant to adversarial attacks," in *6th International Conference on Learning Representations, ICLR 2018, Vancouver, Canada, 2018*. OpenReview.net, 2018. 2, 4, 9, 10

[28] J. Deng, W. Dong, R. Socher, L.-J. Li, K. Li, and L. Fei-Fei, "ImageNet: A large-scale hierarchical image database," in *2009 IEEE Conference on Computer Vision and Pattern Recognition*, 2009, pp. 248–255. 2, 3, 4

[29] A. Kolesnikov, L. Beyer, X. Zhai, J. Puigcerver, J. Yung, S. Gelly, and N. Houlsby, "Big transfer (BiT): General visual representation learning," in *Computer Vision - ECCV 2020 - 16th European Conference, Glasgow, UK, August 23-28, 2020, Proceedings, Part V*, ser. Lecture Notes in Computer Science, vol. 12350. Springer, 2020, pp. 491–507. 2

[30] F. Croce and M. Hein, "Reliable evaluation of adversarial robustness with an ensemble of diverse parameter-free attacks," in *Proceedings of the 37th International Conference on Machine Learning, ICML 2020, 13-18 July 2020, Virtual Event*, ser. Proceedings of Machine Learning Research, vol. 119. PMLR, 2020, pp. 2206–2216. 2, 4, 10

[31] N. Carlini and D. Wagner, "Towards evaluating the robustness of neural networks," in *2017 ieee symposium on security and privacy (sp)*. IEEE, 2017, pp. 39–57. 2, 4, 9, 10

[32] Y. Dong, F. Liao, T. Pang, H. Su, J. Zhu, X. Hu, and J. Li, "Boosting adversarial attacks with momentum," in *2018 IEEE Conference on Computer Vision and Pattern Recognition, CVPR 2018, Salt Lake City, UT, USA, June 18-22, 2018*. Computer Vision Foundation / IEEE Computer Society, 2018, pp. 9185–9193. 2

[33] A. Athalye, N. Carlini, and D. A. Wagner, "Obfuscated gradients give a false sense of security: Circumventing defenses to adversarial examples," in *Proceedings of the 35th International Conference on Machine Learning, ICML 2018, Stockholmsmässan, Stockholm, Sweden, July 10-15, 2018*, ser. Proceedings of Machine Learning Research, vol. 80. PMLR, 2018, pp. 274–283. 2, 5

[34] D. Hendrycks and K. Gimpel, "Gaussian error linear units (GELUs)," *CoRR*, vol. abs/1606.08415, 2016. 3

[35] R. Wightman, "Pytorch image models," https://github.com/rwightman/pytorch-image-models, 2019. 4

[36] S. Xie, R. B. Girshick, P. Dollár, Z. Tu, and K. He, "Aggregated residual transformations for deep neural networks," in *2017 IEEE Conference on Computer Vision and Pattern Recognition, CVPR 2017, Honolulu, HI, USA, July 21-26, 2017*. IEEE Computer Society, 2017, pp. 5987–5995. 4

[37] Z. Li, W. Yang, S. Peng, and F. Liu, "A survey of convolutional neural networks: Analysis, applications, and prospects," *CoRR*, vol. abs/2004.02806, 2020. 4

[38] N. Papernot, P. McDaniel, S. Jha, M. Fredrikson, Z. B. Celik, and A. Swami, "The limitations of deep learning in adversarial settings," in *2016 IEEE European symposium on security and privacy (EuroS&P)*. IEEE, 2016, pp. 372–387. 4, 7

[39] S.-M. Moosavi-Dezfooli, A. Fawzi, O. Fawzi, and P. Frossard, "Universal adversarial perturbations," in *Proceedings of the IEEE conference on computer vision and pattern recognition*, 2017, pp. 1765–1773. 4, 10

[40] M. Andriushchenko, F. Croce, N. Flammarion, and M. Hein, "Square attack: a query-efficient black-box adversarial attack via random search," in *European Conference on Computer Vision*. Springer, 2020, pp. 484–501. 4, 10

[41] J. Chen and Q. Gu, "Rays: A ray searching method for hard-label adversarial attack," in *Proceedings of the 26th ACM SIGKDD International Conference on Knowledge Discovery & Data Mining*, 2020, pp. 1739–1747. 4, 10

[42] J. Kantipudi, S. R. Dubey, and S. Chakraborty, "Color channel perturbation attacks for fooling convolutional neural networks and a defense against such attacks," *IEEE Transactions on Artificial Intelligence*, vol. 1, no. 2, pp. 181–191, 2020. 4

[43] F. Croce and M. Hein, "Minimally distorted adversarial examples with a fast adaptive boundary attack," in *International Conference on Machine Learning*. PMLR, 2020, pp. 2196–2205. 4

[44] W. Xu, D. Evans, and Y. Qi, "Feature squeezing: Detecting adversarial examples in deep neural networks," in *25th Annual Network and Distributed System Security Symposium, NDSS 2018, San Diego, California, USA, February 18-21, 2018*. The Internet Society, 2018. 4

[45] C. Guo, M. Rana, M. Cissé, and L. van der Maaten, "Countering adversarial images using input transformations," in *6th International Conference on Learning Representations, ICLR 2018, Vancouver, BC, Canada, April 30 - May 3, 2018, Conference Track Proceedings*. OpenReview.net, 2018. 4

[46] G. K. Dziugaite, Z. Ghahramani, and D. M. Roy, "A study of the effect of JPG compression on adversarial images," *CoRR*, vol. abs/1608.00853, 2016. 4, 5

[47] N. Das, M. Shanbhogue, S. Chen, F. Hohman, L. Chen, M. E. Kounavis, and D. H. Chau, "Keeping the bad guys out: Protecting and vaccinating deep learning with JPEG compression," *CoRR*, vol. abs/1705.02900, 2017. 4, 5

[48] A. Graese, A. Rozsa, and T. E. Boult, "Assessing threat of adversarial examples on deep neural networks," in *2016 15th IEEE International Conference on Machine Learning and Applications (ICMLA)*. IEEE, 2016, pp. 69–74. 4, 5

[49] D. L. Donoho and J. M. Johnstone, "Ideal spatial adaptation by wavelet shrinkage," *biometrics*, vol. 81, no. 3, pp. 425–455, 1994. 4

[50] A. Chambolle, "An algorithm for total variation minimization and applications," *Journal of Mathematical imaging and vision*, vol. 20, no. 1, pp. 89–97, 2004. 5

[51] A. Athalye, L. Engstrom, A. Ilyas, and K. Kwok, "Synthesizing robust adversarial examples," in *International conference on machine learning*. PMLR, 2018, pp. 284–293. 5

[52] R. R. Selvaraju, M. Cogswell, A. Das, R. Vedantam, D. Parikh, and D. Batra, "Grad-CAM: Visual explanations from deep networks via gradient-based localization," *International Journal of Computer Vision*, vol. 128, no. 2, p. 336–359, Oct 2019. 5

[53] G. Ortiz-Jiménez, A. Modas, S. Moosavi-Dezfooli, and P. Frossard, "Hold me tight! influence of discriminative features on deep network boundaries," in *Advances in Neural Information Processing Systems 33: NeurIPS 2020, December 6-12, 2020, virtual*, 2020. 5, 8

[54] S. A. Fezza, Y. Bakhti, W. Hamidouche, and O. Déforges, "Perceptual evaluation of adversarial attacks for cnn-based image classification," in *2019 Eleventh International Conference on Quality of Multimedia Experience (QoMEX)*. IEEE, 2019, pp. 1–6. 5, 6

[55] Z. Wang, A. C. Bovik, H. R. Sheikh, and E. P. Simoncelli, "Image quality assessment: from error visibility to structural similarity," *IEEE transactions on image processing*, vol. 13, no. 4, pp. 600–612, 2004. 5, 6

[56] E. C. Larson and D. M. Chandler, "Most apparent distortion: full-reference image quality assessment and the role of strategy," *Journal of electronic imaging*, vol. 19, no. 1, p. 011006, 2010. 5, 6

[57] J. Gildenblat and contributors, "Pytorch library for CAM methods," https://github.com/jacobgil/pytorch-grad-cam, 2021. 5

[58] Y. Sharma, G. W. Ding, and M. A. Brubaker, "On the effectiveness of low frequency perturbations," in *Proceedings of the Twenty-Eighth International Joint Conference on Artificial Intelligence, IJCAI 2019, Macao, China, August 10-16, 2019*. ijcai.org, 2019, pp. 3389–3396. 5